THE GEOLOGICAL SOCIETY OF AMERICA®

A comprehensive genetic model for the world's largest Sb deposit (Xikuangshan, China)

Shanling Fu[1], Ruizhong Hu[1,2,†], Jiantang Peng[1], Liyan Wu[1], and Dongsheng Ma[3]
[1]*State Key Laboratory of Ore Deposit Geochemistry, Institute of Geochemistry, Chinese Academy of Sciences, Guiyang 550081, China*
[2]*College of Earth and Planetary Sciences, University of Chinese Academy of Sciences, Beijing 100049, China*
[3]*School of Earth Sciences and Engineering, Nanjing University, Nanjing 210023, China*

ABSTRACT

The Mesozoic (160–130 Ma), fault-controlled Xikuangshan Sb deposit within Devonian limestone strata of Hunan Province, Southern China is the world's largest Sb deposit containing a proven reserve of ~2.5 m Sb. Although mined for over a century, its genesis remains poorly understood. Here we use new He-Ar isotope data of hydrothermal stibnite and both new and existing C-O-Sr-Nd isotopes of hydrothermal calcite with known stages to decipher its genesis and the major constraints on mineralization intensity. The $^{3}He/^{4}He$ and $^{40}Ar/^{36}Ar$ ratios of fluid inclusions trapped in stibnite are from 0.01 to 0.04 Ra (Ra: atmospheric $^{3}He/^{4}He$ ratio) and 304–1077, respectively, indicating the ore-forming fluids at Xikuangshan were dominated by air-saturated meteoric groundwater after interaction with crustal rocks. Ore-stage calcite C and O isotopes indicated that most CO_2 in the fluids was acquired from marine carbonate rocks by dissolution; whereas Sr and Nd isotopes differed from deposited Devonian country rocks but were similar to the underlying regional Proterozoic clastic rocks in the region. Calcite from early and late stages showed a strong positive correlation between $\delta^{18}O$ and $^{87}Sr/^{86}Sr$, consistent with the mixing between the circulating groundwater and compounds released from the Proterozoic rocks due to extensive fluid-rock interaction. The $^{3}He/Q$ ratios of the fluid inclusions are low, varying from 4.3 to 18.5 × 10^{-15} cm^3 standard temperature and pressure (STP) J^{-1}, indicating deep-seated magma could have provided heat by conduction but no volatiles into the ore-forming fluids. Based on these new results, we suggest that deep-seated granitic magma heated the down-going meteoric groundwater along fault zones, after which the groundwater extensively interacted with and extracted Sb from the Proterozoic Sb-rich rocks to form Sb-rich fluids. The Sb-rich fluids then ascended through regional faults and deposited Sb as stibnites at favorable structural traps to form the Xikuangshan Sb deposit. This study highlights that extensive water-rock interaction is essential to form the deposit, and more intensive water-rock interaction at an early stage allowed for early-stage mineralization yielding higher Sb reserves (>80%) at Xikuangshan.

INTRODUCTION

The giant Xikuangshan Sb deposit, situated in Hunan Province, Southern China, was discovered in 1541, first mined in 1892, and has since become one of the most important global providers of Sb resource. This is the world's largest Sb deposit, containing a proven reserve of ~2.5 m Sb, with an average Sb grade of 4% (Hu et al., 2017). Though extensively studied since the early 1920s (Tegengren, 1921), the genesis of this deposit remains controversial. Based on its distance from exposed intrusive rocks, Wang et al. (1938) regarded it as a distal magmatic hydrothermal deposit. In the early 1980s, it was classified as a stratabound deposit, with Sb derived from the host strata (Tu, 1984; Xiao and Li, 1984). Based on geochemical and geophysical data, some researchers suggested that this deposit is related to igneous rocks at depth or underlying Proterozoic basement rocks (Liu et al., 1985; Li, 1996; Jin et al., 1999; Peng et al., 2001; Ma et al., 2002, 2003). In addition, a syngenetic-exhalation model and a sedimentary-diagenetic model have also been proposed for this deposit (Zhang et al., 1998; Fan et al., 2004). The mineralization stages of the deposit have been split, where >80% of the total Sb reserves in the deposit were produced in the early stage (Wen et al., 1993; Hu and Peng, 2018); however, little is known about why the mineralization during this stage is so much more extensive.

Accordingly, a combined He-Ar-C-O-Sr-Nd isotope comparison analysis on hydrothermal minerals, notably lacking from previous studies, could help resolve the debates surrounding the origin and mineralization intensity of the deposit. Helium-Ar isotopes of fluid inclusions trapped by hydrothermal sulfides have proven to be good tracers of water-rock interaction and heat source. These isotopes also act as an effective mechanism for tracing the source of ore-forming fluids due to significant differences in $^{3}He/^{4}He$ and $^{40}Ar/^{36}Ar$ ratios between fluids derived from different geochemical reservoirs (Turner et al., 1993). For example, the >100-fold difference between $^{3}He/^{4}He$ ratios of upper mantle (6–9 Ra, where Ra is the atmospheric $^{3}He/^{4}He$ ratio, 1.39×10^{-6}) and the crust (0.01–0.05 Ra) offers unique insight into processes where mantle or magmatic volatiles have been added to crustal fluids (Stuart et al., 1995; Burnard and Polya, 2004; Hu et al., 2009, 2012; Davidheiser-Kroll et al., 2014; Wu et al., 2018). Carbon and O isotopes of the associated hydrothermal calcites are also effective tracers for origin of the ore-forming fluids and the intensity of water-rock interaction (Ohmoto, 1986; Hoefs, 1987; Wulff et al., 2010; Jaguin et al., 2014). Alternatively, the Sr-Nd and Sr-O isotopes of ore-stage minerals, such as calcite in the Xikuangshan Sb deposit, can be used to evaluate fluid-rock interaction in a dynamic hydrothermal fluid system (Johnson and McCulloch, 1995; Savard and Kontak, 1998; Voicu et al., 2000; Peng et al., 2003b, 2008; Sánchez et al., 2010); however, no such study on He-Ar isotopes for the Xikuangshan Sb deposit was previously performed to date, and the published C-O-Sr-Nd data of hydrothermal calcites from this deposit are either limited in extent or without known stages. With these in mind, the present study used new He-Ar-C-O-Sr-Nd and existing C-O-Sr-Nd isotope data of hydrothermal minerals with known stages to reveal the

[†]Corresponding author: huruizhong@vip.gyig.ac.cn.

GSA Bulletin; March/April 2023; v. 135; no. 3/4; p. 1074–1088; https://doi.org/10.1130/B36424.1; 12 figures; 4 tables.
published online 25 July 2022

origin and primary constraints on mineralization intensity of the giant Xikuangshan Sb deposit. Antimony concentrations of different types of regional rocks from previous studies are also included in the discussion, as such comprehensive data sets allowed the proposal of a new genetic model for this giant deposit.

GEOLOGY

Regional Geology

The South China Block (SCB) in the southeastern Eurasian continent consists of the Yangtze Block in the northwest and the Cathaysian Block in the southeast (Fig. 1A), which were amalgamated along the Jiangshao suture at ca. 830 Ma (Zhao et al., 2011). The giant Xikuangshan Sb deposit is located in the Xiangzhong (central Hunan Province) Basin in the southeastern part of the Yangtze Block. This basin is bounded by the Xuefengshan Uplift Belt to the northwest (Fig. 1B). Rocks exposed in this region are composed of the Proterozoic metamorphic basement occurring along the Xuefengshan Uplift Belt (Fig. 1B) and Paleozoic–Mesozoic sedimentary cover, with Cenozoic sediments in some areas (Wang et al., 2013).

The Proterozoic metamorphic basement mainly comprises the Lengjiaxi and Banxi Groups, which were overlain unconformably by Ediacaran–Cambrian sequences, and to a lesser degree, the Late Paleozoic sequence (Figs. 1B and 2). The Lengjiaxi Group is mainly composed of slate, siltstone and sandstone, plus minor amounts of conglomerates and flysch turbidite (total thickness >2500 m). Mafic-ultramafic intrusive rocks and bimodal volcanic rocks are also present in this group (Zhou et al., 2002). The overlying Banxi Group consists of the lower Madiyi Formation and the upper Wuqiangxi Formation (Fig. 2). The major rock types of this group are gray-green and purplish-red graywacke, siltstone, sandy slate, and slate (total thickness, 1000–6000 m; Fig. 2; HBGMR, 1988). Regionally, the sedimentary rocks of Ediacaran–Early Paleozoic consist of silicalite, argillite, sandstone, siltstone, and minor tuffaceous slate beds (total thickness, 2000–7000 m; Fig. 2; Yang et al., 2006). The Xiangzhong Basin is unconformably developed on the top of the pre-Devonian sequences (Lengjiaxi and Banxi Groups and Ediacaran to Early Paleozoic sedimentary rocks). Continuous sedimentation from Middle Devonian to Early Triassic produced 1500–9000 m of carbonates and clastic sedimentary rocks, such as limestone, sandstone, shale, and conglomerate, in the basin (Fig. 2).

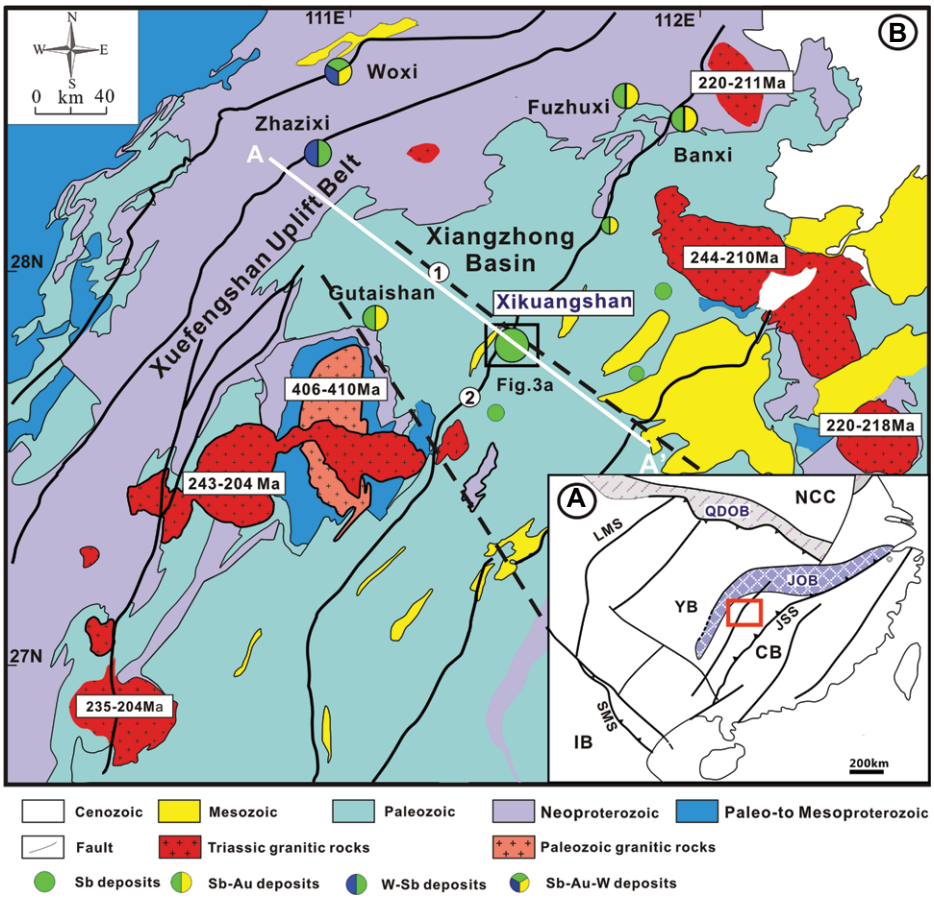

Figure 1. (A) Tectonic framework of South China Block showing the location of central Hunan (Xiangzhong) (modified from Qiu et al., 2016; Hu et al., 2017). (B) Regional geological map of the central Hunan, South China showing the distribution of important Sb deposits (modified from HBGMR, 1988; Xie et al., 2019). Age data for granites are sourced from Wang et al. (2007), Wang et al. (2012), Li et al. (2014), Fu et al. (2015), and Xie et al. (2019). CB—Cathaysia Block; IB—Indochina Block; JOB—Jiangnan Orogen Belt; JSS—Jiang-Shao Suture; LMS—Longmenshan fault; NCC—North China Craton; QDOB—Qinling-Dabie Orogen Belt; SMS—Song-Ma Suture; YB—Yangtze Block; ①—Xikuangshan-Lianyuan fault; ②—Chengbu-Taojiang fault; A–A′—location of Figure 12.

Several tectonic events took place in this region at various times, including the middle Paleozoic, early Mesozoic, and late Mesozoic, since the Neoproterozoic amalgamation of Yangtze and Cathaysian Blocks (Faure et al., 2009; Charvet, 2013; Wang et al., 2013). The Middle Paleozoic tectonic event, commonly referred to as the Caledonian orogeny, was responsible for the development of the angular unconformities between the Lower Silurian and Middle Devonian strata in the basin (Fig. 2; Shu, 2006; Wang et al., 2013), as well as the deformation of the pre-Devonian strata, such as folding, shearing, faulting, and uplift (Shu et al., 2009; Chu et al., 2012a, 2012b). This tectonic event also produced abundant granitic rocks with ages from ca. 450–350 Ma (Fig. 1B), while the early Mesozoic tectonic event or the Indosinian orogeny produced more widespread granitic plutons (Wang et al., 2013), with granite ages varying from 255 to 200 Ma across the entire SCB and from 244 to 204 Ma in the Xiangzhong district (Fig. 1B; Wang et al., 2013; Fu et al., 2015; Lu et al., 2017). It is suggested that the Indosinian granitoids are related to the westward subduction of the paleo-Pacific plate underneath the Eurasian continent (Li and Li, 2007) or the continental collision between the SCB and the Indochina Block to the west in response to the closure of the Paleotethys (Lepvrier et al., 2004; Wang et al., 2013). The late Mesozoic tectonic event (i.e., Yanshanian event) is responsible for the formation of a large granite province covering much of the Cathaysia Block (Li and Li, 2007; Wang et al., 2013). The Yanshanian granitic rocks were dominantly emplaced from the Jurassic to Cretaceous (160–140 Ma; Mao et al., 2013; Wang et al., 2013) and related to either lithospheric

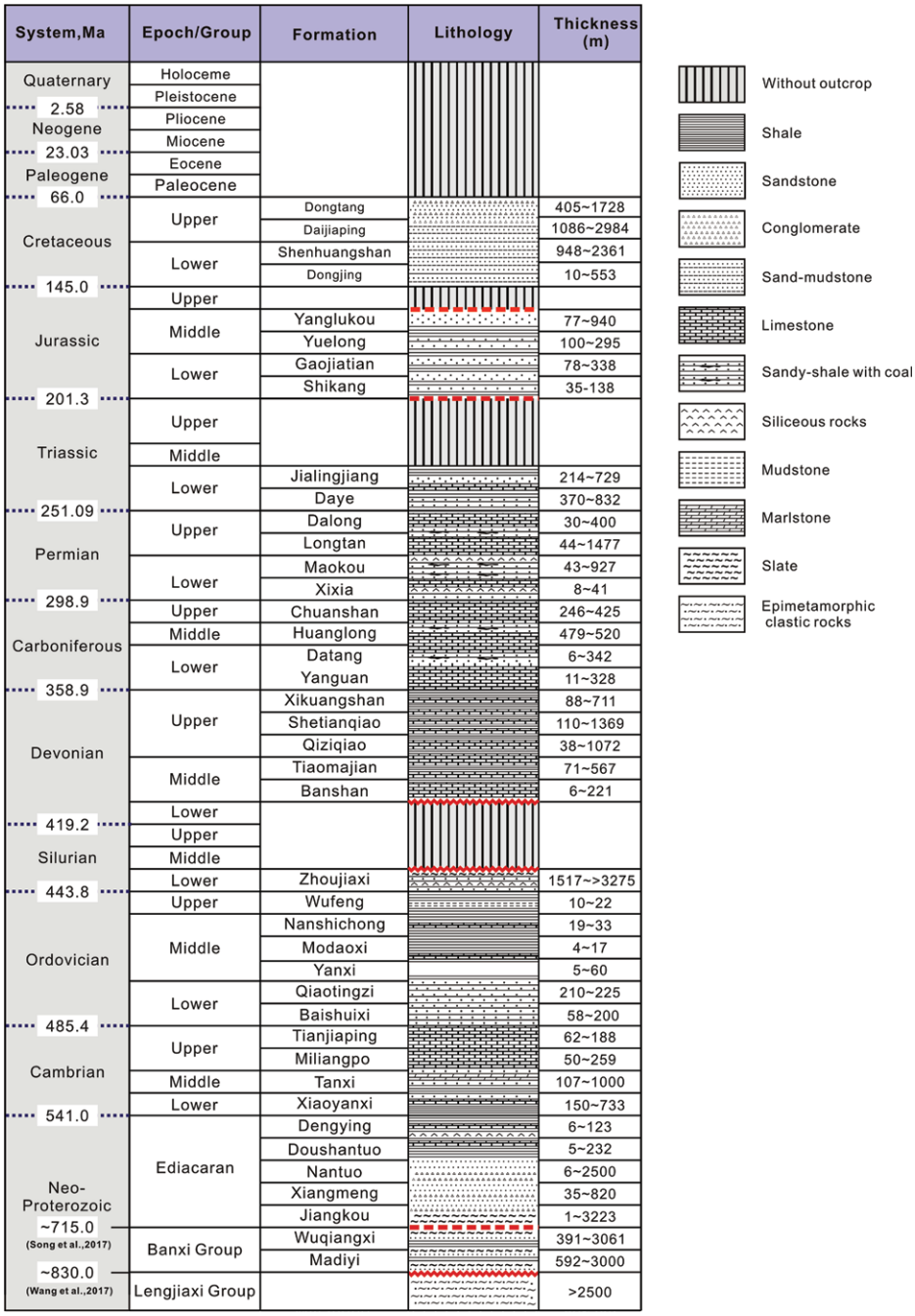

Figure 2. Stratigraphic columns of the central Hunan Province including the Xuefengshan Uplift Belt and Xiangzhong Basin (modified after HBGMR, 1988).

extension and associated asthenosphere upwelling in an intraplate setting (Wang et al., 2013) or the westward subduction of the Pacific plate beneath the Cathaysia Block (Li and Li, 2007). Although no substantial Yanshanian granites have been identified in the Xiangzhong district, sparse patches have intruded into the Late Triassic granites around the Xiangzhong Basin (Ding et al., 2006; Chen et al., 2007; Liu et al., 2013), indicating that there might be substantial Yanshanian granites in the depth of those Late Triassic granites (Hu et al., 2021). Extensive gravity abnormalities within the Xiangzhong Basin further suggest there might be buried Yanshanian granites in this region (Rao et al., 1999; Zhu, 2004).

More than 100 Sb-bearing deposits have been found in this region (Hu et al., 2017), all of which can be divided into two groups based on metal association, as well as lithological control: Group A hosted in the late Paleozoic carbonates and clastic rocks within the Xiangzhong Basin and Group B associated with the Proterozoic low-grade metamorphosed clastic rocks in the Xuefengshan Uplift Belt and Xiangzhong Basin (Ma et al., 2002). Group A is dominated by Sb-only deposits, which are commonly distal to known granitic intrusions in the region and occur as stratiform, as represented by the giant Xikuangshan Sb deposit (Fig. 1B; Fan et al., 2004; Hu and Peng, 2018). In these deposits, stibnite is the only ore mineral. Group B deposits are polymetallic (Fig. 1B), as represented by the Woxi Sb-Au-W (Zhu and Peng, 2015), Zhazixi Sb-W (Peng et al., 2010; Zeng et al., 2017a, 2017b), and the Longshan Sb-Au deposits (Fu et al., 2016; Zhang et al., 2019). The mineralization occurred as veins, mainly confined to the weakly metamorphosed clastic rocks of Proterozoic ages. The ore minerals include stibnite, native gold, pyrite, arsenopyrite, and scheelite.

Deposit Geology

The giant Xikuangshan Sb deposit is located at the intersection of the NE-striking Taojiang-Chengbu and NW-striking Xikuangshan-Lianyuan major faults (Fig. 1B). The exposed sedimentary strata in the region are mainly Upper Devonian Xikuangshan Formation (D_3x) and Shetianqiao Formation (D_3s) and Lower Carboniferous Datang Formation (C_1d) and Yanguan Formation (C_1y; Fig. 3). The Xikuangshan Formation is composed of interbedded carbonate and shale, with a hematite layer (Fig. 3B). Most important Sb mineralization is present in the middle portion of the Shetianqiao Formation (D_3s^2), and to a lesser extent, the lower part of this Formation (D_3s^1). The D_3s^2 is composed of sandstone, carbonate and mudstone layers from the bottom to the top (total thickness >350 m). The carbonate layer is primarily composed of limestone interlayered with thin shale or sandy mudstone, and hosts the bulk of Sb mineralization. The ore-bearing carbonate layer is overlain by a layer of shale and/or mudstone, which was considered to be a fluid barrier during the hydrothermal mineralization (Jin et al., 2001; Yang et al., 2006).

Structurally, the Xikuangshan deposit is strictly confined within the NE-trending Xikuangshan composite anticline consisting of four smaller anticlines that all contain important orebodies (Fig. 3A; Laokuangshan, Tongjiayuan, Feishuiyan, and Wuhua). The composite anticline was cut by several NE-trending faults; among them, the fault F_{75} is a part of the NE-striking Chengbu-Taojiang regional fault that cut the northwest limb of the anticline. This fault formed in the Triassic as a thrust and

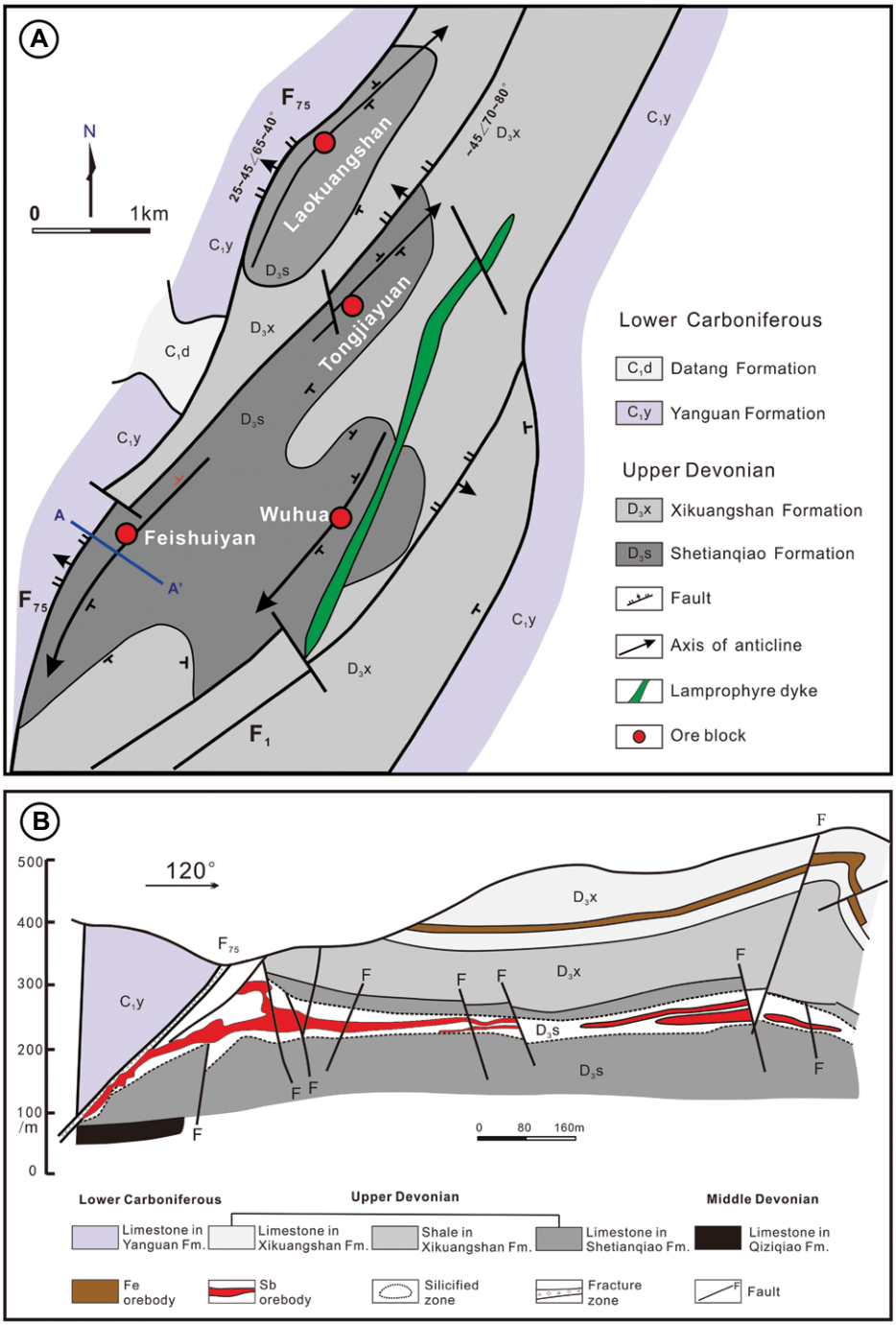

Figure 3. (A) Simplified geological map of the Xikuangshan Sb deposit (modified after Peng and Hu, 2001). (B) A–A′ profile of the Xikuangshan Sb deposit showing the shapes and distribution of orebodies in the Xikuangshan deposit (modified after Tao et al., 2002).

reactivated in the Jurassic to a normal fault (Li et al., 2013), and it was thought to be the main pathway of the ore-forming fluids, which is demonstrated by the occurrence of Sb mineralization in the immediate footwall of this fault and increasing intensity of hydrothermal alteration such as silicification toward the fault (Liu and Jian, 1983).

A NNE-trending lamprophyre dike that occurs in the eastern part of the deposit is the only exposed intrusion in the deposit area (Fig. 3A) and was considered to postdate the Xikuangshan Sb deposit (Wu and Hu, 2000). K-Ar dating of biotite and K-feldspar in this dike yielded 127.8 Ma and 118.4 Ma, respectively (Wu and Hu, 2000). Moreover, granitic xenoliths were found in the dike (Wu and Hu, 2000), suggesting the presence of buried granites at the depth of the Xikuangshan deposit area. Considering the ages of the lamprophyre dike and geophysical data, these buried granites may have formed during the Yanshanian (Li, 1996; Rao et al., 1999).

The host rocks, mainly the carbonates of the Devonian Shetiaoqiao Formation, were variably silicified in the fractures, with increasing intensity toward the regional fault F_{75}. The Sb orebodies are associated with intensive silicification and were spatially controlled by the interlayer fault zones, thus appearing to be stratiform in distribution (Fig. 3B); however, at a smaller scale, a single orebody contains multiple veins that form irregular networks, consistent with a fractured zone (Fig. 4). Each orebody measures 30–600 m in length along strike and 1–5 m (locally up to 20 m) in thickness (Fig. 3). The ore grades vary from 3.5 to 5.7 wt% Sb, with an average of 4.0 wt% Sb (Kuang, 2000).

The common ore textures are massive, brecciated, disseminated, strip and network-like (Figs. 4 and 5). Stibnite is the only ore mineral, while quartz and calcite are the main gangue minerals. Minor amounts of pyrite, fluorite, barite, and talc are present locally. Based on mineral assemblages, the ores can be divided into quartz-stibnite, calcite-quartz-stibnite, and calcite-stibnite types. The quartz-stibnite type of ores represents >80% of the Sb reserves of the deposit (Wen et al., 1993; Hu and Peng, 2018). Alternatively, the mineral paragenesis can be divided into three stages of early, late, and post-mineralization (Fig. 6). The mineral assemblage of the early mineralization stage is mainly composed of quartz and stibnite, with minor calcite. Stibnite is present in massive ores (Fig. 5A), disseminated ores with quartz (Fig. 5B), as randomly oriented needles in a silicified limestone matrix (Fig. 5C), and as large tabular crystal intergrown with calcite (Figs. 5D and 7A). This stage of mineralization is estimated to produce >80% of the total Sb reserves of the deposit. The late mineralization stage assemblage is composed of calcite and stibnite, with minor quartz and rare fluorite and barite. The calcite crystals are intergrown with acicular and fine-grained stibnite (Figs. 5E–5G and 7B). Postmineralization minerals are mainly coarse-grained calcite (Fig. 5H) that commonly fills the pores or fractures of deformed ores (Fig. 4B).

Nearly all Sb orebodies in the Xikuangshan deposit are strictly confined within the NE-trending Xikuangshan complex anticline that formed during the Mesozoic, placing the Sb mineralization event in the Mesozoic; however, the precise age of the Xikuangshan deposit has not been well constrained due to the lack of suitable minerals for radiometric dating. The ore-stage cal-

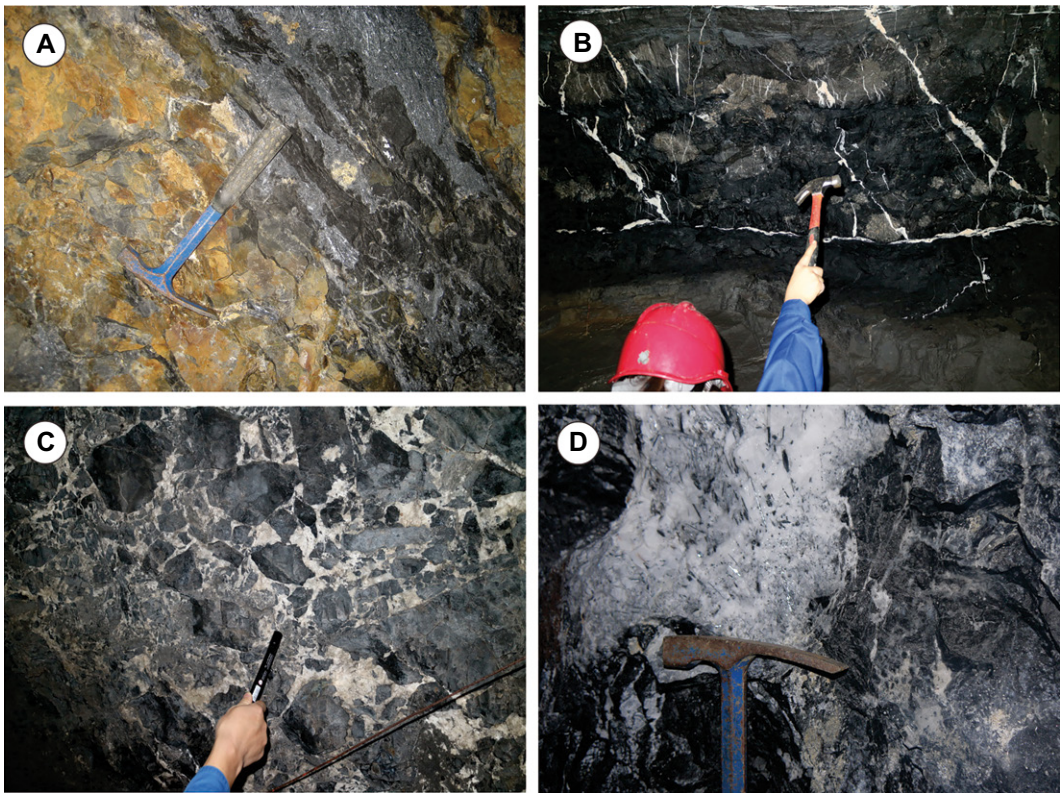

Figure 4. Field photographs of orebodies from the Xikuangshan Sb deposit. (A) Early mineralization stage stibnite-quartz ore veins occurred in Devonian silicified limestone; (B) early- and late-stage ores cut by postmineralization calcite vein; (C) network ore in the brecciated silicified limestone; (D) acicular stibnite disseminated in late stage-calcite vein.

cites in the Xikuangshan have high Sm/Nd ratios and are thought to be suitable for Sm-Nd dating (Peng et al., 2003a, 2004). Using this technique, Peng et al. (2003a) determined that the Xikuangshan Sb deposit was likely formed sometime between 156 Ma and 124 Ma. More recently, Fu et al. (2020) obtained 156–117 Ma (U-Th)/He ages for the zircons in alteration zones of the Xikuangshan deposit, broadly overlapping with the Sm-Nd ages. Similar ages have been obtained for other Sb deposits in the region. For example, Rb-Sr and Sm-Nd isotopes of hydrothermal sulfides and (U-Th)/He isotopes of zircons from altered host rocks yield ca. 130 Ma for the Banxi Sb deposit (Li et al., 2018; Fu et al., 2019). Ar-Ar isotopes of hydrothermal muscovite yield ca. 160 Ma for the Longshan Sb-Au (Zhang et al., 2018). The Mesozoic Sb mineralization event is not restricted to the Xiangzhong district. It also took place in the adjacent Youjiang district to the southwest. For instance, Peng et al. (2003b) reported a Sm-Nd age of ca. 148 Ma for fluorite from the Qinglong Sb deposit in the Youjiang district; Xiao (2014) reported a Sm-Nd isochron age of ca. 131 Ma for calcite from the Banian Sb deposit in the same district. The reported ages of above deposits overlap with those of the Xikuangshan Sb deposit, indicating that Sb mineralization between 160 and 130 Ma may have been extensively developed in the Xiangzhong and Youjiang districts.

The fluid inclusion data indicate that the ore-forming fluids of the Xikuangshan Sb deposit are of low temperatures and salinities (Jin et al., 2001): 140–250 °C and 3–6 wt% NaCl equiv., respectively, for the early stage, and 120–200 °C and 0.3–0.9 wt% NaCl equiv., respectively, for the late stage (Lin, 2014). Thus, the temperatures and salinities decreased during mineralization.

SAMPLES AND ANALYTICAL METHODS

Previously published C-O-Sr-Nd data of hydrothermal calcites from the Xikuangshan Sb deposit are either limited in extent or without known specific stages; therefore, a new set of samples of early and late stages were collected here from several underground mining tunnels of the deposit (Tables 1 and 2) for He-Ar-C -O-Sr-Nd isotope analysis. Hand specimens were crushed to 0.3–0.5 mm fragments for calcite separation and 1–2 mm fragments for stibnite separation, using a binocular microscope. The calcite separates were ground to 200 mesh in an agate mortar, and the powdered calcite samples were used for C-O-Sr-Nd isotope analysis. Because calcite is not a good helium trap (Turner et al., 1993), the stibnite separates were used for He-Ar isotope analysis.

A mass spectrometer (GV 5400) equipped with an online volatile extraction system was used for He and Ar isotope analysis at the Institute of Geology and Geophysics, Chinese Academy of Sciences, Beijing, China. The analytical methods are similar to those described in Stuart et al. (1994, 1995), where ~500–1000 mg of stibnite separates were ultrasonically cleaned in alcohol, dried, and then loaded in online *in vacuo* crusher buckets. The samples were then baked at ~150 °C online with an ultra-high vacuum system for >24 h to remove adhered atmospheric gases. Gases within fluid inclusions were released from the grains into an all-metal extraction system by sequential crushing within modified Nupro-type valves, and the released gases were purified with two SAES Zr-Al getters, one at room temperature and the other at 450 °C. Helium was separated from Ar using activated charcoal at liquid N_2 temperature to trap the Ar, and afterwards, He and Ar isotopes were analyzed on the GV 5400 mass spectrometer. Procedural blanks were $<2 \times 10^{-10}$ cm^3 STP ^4He and (2–4) $10^{-10}cm^3$ STP ^{40}Ar, and constituted <1% of analyses. Gas abundances were measured by peak-height comparison with known amounts of air, and Ar isotopes were calibrated against pipettes of 9.3×10^{-4} cm^3 STP air. Helium calibrations were made on 5.2×10^{-7} cm^3 STP air.

Carbon and O isotope measurements were carried out using the methods described in Walters et al. (1972). CO_2 gas was extracted by react-

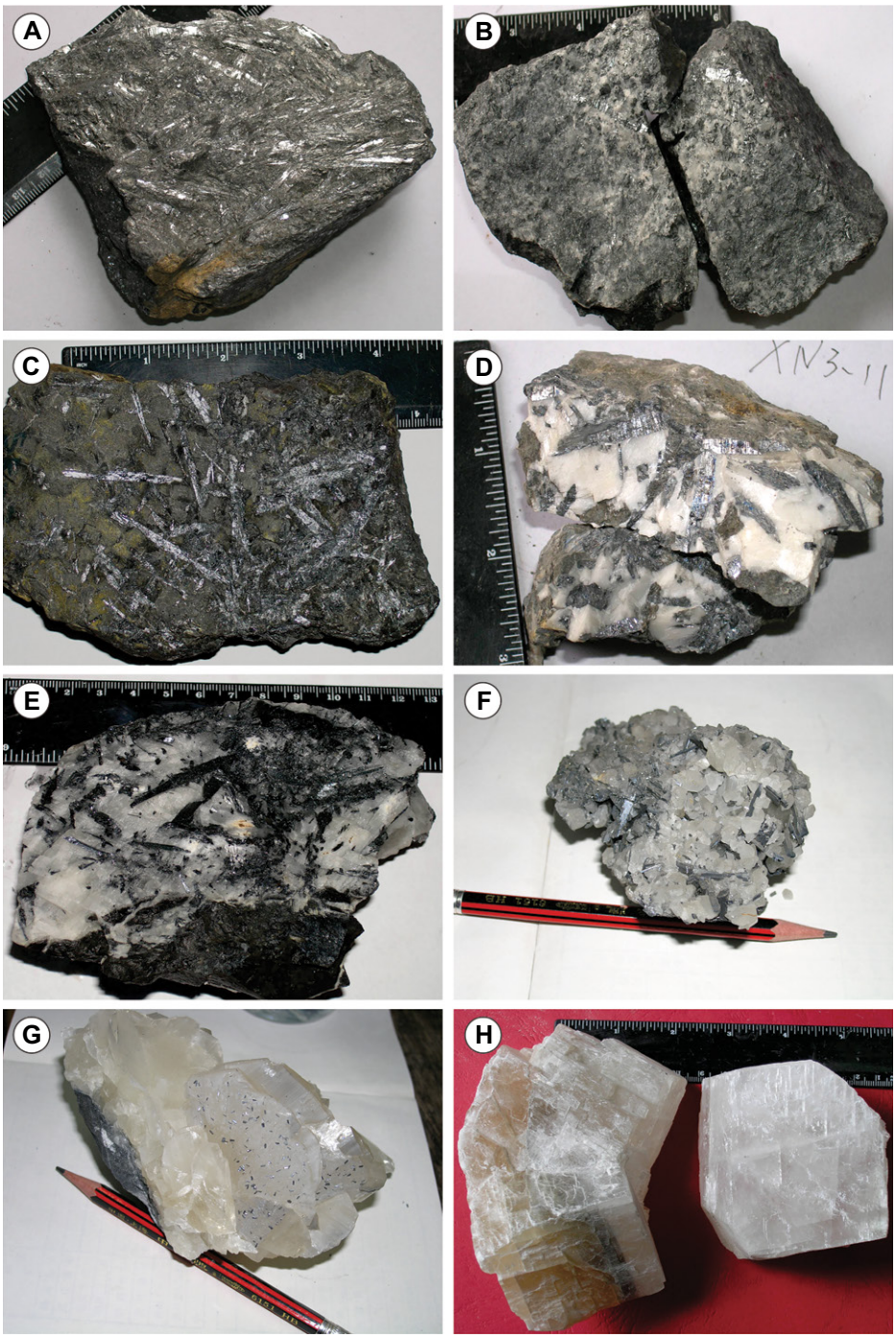

Figure 5. Photographs of hand specimens from the Xikuangshan Sb deposit. (A) Stibnite present in massive ore; (B) stibnite present in disseminated ore with quartz; (C) randomly oriented acicular stibnite in a silicified limestone matrix; (D) large tabular stibnites in early-stage quartz vein; (E and F) acicular stibnite in late-stage calcite vein; (G) fine-grained stibnite in late-stage calcite; (H) postmineralization stage coarse-grained calcite.

ing ~5 mg of carbonate powder for 12 h with phosphoric acid at 25 °C. The liberated gas was analyzed on the MAT-252 mass spectrometer at the Institute of Geochemistry, Chinese Academy of Sciences, Guiyang, China. Carbon and O isotopic compositions are reported in the common δ notation in permil relative to the (WO4406) Peedee belemnite (PDB) and standard mean ocean water (SMOW) standards, respectively. The analytical precision is about ±0.2‰ (2σ).

Rubidium, Sr, Sm, and Nd concentrations, as well as Sr-Nd isotopic compositions were measured using a MAT-261 mass spectrometer at the Tianjin Institute of Geology and Mineral Resources, Chinese Academy of Geological Sciences. Two separate sample solution aliquots were prepared: one for the determination of Rb, Sr, Sm, and Nd concentrations and the other to measure the $^{87}Sr/^{86}Sr$ and $^{143}Nd/^{144}Nd$ ratios. The elemental abundances were determined by isotope dilution, whereas the $^{87}Sr/^{86}Sr$ and $^{143}Nd/^{144}Nd$ ratios were measured from unspiked solutions of pre-concentrated sample splits. Procedural blanks used in the Rb-Sr isotope analyses are ~50 pg for Rb and Sr. The measured Sr isotopic ratios were normalized to an $^{86}Sr/^{88}Sr$ of 0.1194. The National Bureau of Standards (NBS) 987 standard (recommended $^{87}Sr/^{86}Sr = 0.710249$, Thirlwall, 1991) was used for instrument calibration. Procedural blanks used in the Sm-Nd isotope analyses are 30 pg for Sm and 54 pg for Nd. The Johnson and Mattey Nd standard, with a recommended $^{143}Nd/^{144}Nd$ ratio of 0.511132 ± 5 (Su et al., 2009), was used for instrument calibration. The measured Nd isotopic ratios were normalized to $^{146}Nd/^{144}Nd$ of 0.7219, using the power law fractionation correction. The errors of reproducibility of the isotopic ratios are less than 0.005% (2σ); the precision for Sm and Nd concentrations are less than 0.1% deviation (2σ) from the recommended values. The BCR-1 reference used in this study yielded 6.57 ppm Sm, 28.75 ppm Nd, and an average $^{143}Nd/^{144}Nd$ ratio of 0.512644 ± 5, notable within the ranges of recommended values (0.512650 ± 40, Jahn et al., 1980; 0.512629 ± 8, Raczek et al., 2003).

ANALYTICAL RESULTS

Helium-Argon Isotopes

Helium and Ar isotopic and abundance data of fluid inclusions trapped in stibnite from the Xikuangshan Sb deposit are presented in Table 1. The concentrations of ^{4}He and ^{40}Ar range from 1.4×10^{-7} to 97.5×10^{-7} cm^3 STP g^{-1} and 2.6×10^{-7} to 86.0×10^{-7} cm^3 STP g^{-1}, respectively. Compared with the late-stage stibnite, both the ^{4}He and ^{40}Ar concentrations in fluid inclusions trapped by the early-stage stibnite were generally higher. The $^{3}He/^{4}He$ ratios vary narrowly from 0.01 to 0.03 Ra (average, 0.02 Ra). The $^{40}Ar/^{36}Ar$ ratios vary from 304 to 1077 (average, 365), which is slightly higher than the atmospheric value of 296 (Hu et al., 1998a; Burnard et al., 1999). The co-variation of He-Ar isotopes is illustrated in Figure 8.

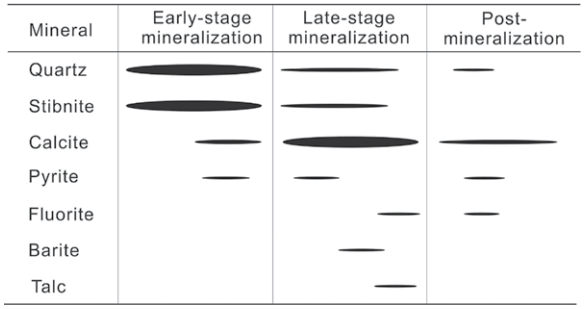

Figure 6. A paragenetic sequence of minerals from the Xikuangshan Sb deposit.

Carbon-Oxygen Isotopes

The C-O isotopic compositions of hydrothermal calcites from the Xikuangshan Sb deposit are listed in Table 2. The calcites of the early and late mineralization stages yielded $\delta^{13}C$ values ranging from −8.2‰ to −4.3‰, and +0.6‰ to +2.1‰, respectively, whereas the $\delta^{18}O$ values of these two calcite types ranged from +17.8‰ to +18.6‰ and +15.3‰ to +17.1‰, respectively. The co-variation of the C-O isotopes is illustrated in Figure 9.

Rubidium-Strontium Isotopes

The concentrations and Rb-Sr isotopes of hydrothermal calcites from the Xikuangshan Sb deposit are given in Table 3. Overall, the late-stage calcites have higher Rb contents than those in the early stage. Strontium contents in the late-stage calcites (less than 210 ppm) are much lower than those in the early stage (642–815 ppm). The $^{87}Sr/^{86}Sr$ ratios of the early-stage calcites vary narrowly from 0.71212 to 0.71282 (average, 0.7125). In contrast, the $^{87}Sr/^{86}Sr$ ratios of late-stage calcites vary more significantly from 0.71018 to 0.71241 (average, 0.7108), which is slightly lower than that of the early-stage calcites.

Samarium-Neodymium Isotopes

The Sm-Nd isotopic compositions of hydrothermal calcites from the Xikuangshan Sb deposit are listed in Table 4. The calcites formed at different stages have contrasting $^{147}Sm/^{144}Nd$ and $^{143}Nd/^{144}Nd$ ratios. Early-stage calcites have $^{147}Sm/^{144}Nd$ values of 0.9411–8.4197 and $^{143}Nd/^{144}Nd$ values of 0.51260–0.52021; whereas late-stage calcites had lower $^{147}Sm/^{144}Nd$ values of 0.0890–0.6017 and $^{143}Nd/^{144}Nd$ values of 0.51178–0.51220.

DISCUSSION

Ore-Forming Fluids Source and Water-Rock Interaction

The source of ore-forming fluids for the Xikuangshan deposit has long been a matter

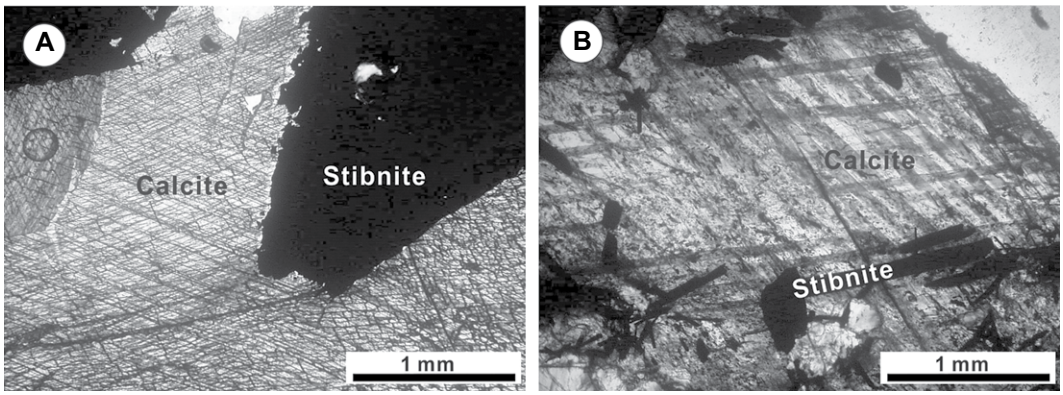

Figure 7. Photomicrographs of thin sections from the Xikuangshan Sb deposit. (A) Early-stage calcite intergrown with coarse-gained stibnite, crossed polars; and (B) late-stage calcite intergrown with fine-grained acicular stibnite, crossed polars.

TABLE 1. HELIUM AND ARGON ISOTOPE DATA OF FLUID INCLUSIONS TRAPPED BY HYDROTHERMAL STIBNITE FROM THE XIKUANGSHAN ANTIMONY DEPOSIT

Sample	Mineral	Location and elevation (m)	Weight (g)	^{4}He ($10^{-7}cm^3STP/g$)	^{40}Ar ($10^{-7}cm^3STP/g$)	$^{3}He/^{4}He$ (Ra)	±	$^{40}Ar/^{36}Ar$	±	$^{40}Ar^*/^{4}He$ (10^{-3})	$^{3}He/Q$ (10^{-15} cm^3 STP J^{-1})
Early-stage											
XKS-1-6	Stibnite	Level #1, Laokuangshan, +350	0.5467	97.5	86.0	0.021	0.010	1077	12	637	17.7
XKS-3-3	Stibnite	Level #3, Laokuangshan, +300	0.4362	10.8	3.12	0.022	0.010	311	3	11	16.7
XKS-7-1	Stibnite	Level #7, Laokuangshan, +190	0.7793	16.4	7.95	0.011	0.005	307	3	13	4.73
XKS-9-3	Stibnite	Level #9, Laokuangshan, +170	0.7536	30.4	6.41	0.014	0.002	311	3	8	18.5
XKS-9-5	Stibnite	Level #9, Laokuangshan, +170	0.6162	11.3	8.71	0.021	0.010	304	3	13	5.70
XKS-13-8	Stibnite	Level #13, Laokuangshan, +78	0.7104	9.9	3.38	0.020	0.009	313	4	15	12.9
XKS-5-1	Stibnite	Level #5, Tongjiayuan, +250	0.6800	14.2	5.64	0.015	0.001	310	5	15	9.66
XKS-6-3	Stibnite	Level #6, Tongjiayuan, +210	0.4263	11.0	4.07	0.019	0.009	316	4	20	11.6
Late-stage											
XKS-5-6	Stibnite	Level #5, Tongjiayuan, +250	0.5272	5.7	4.19	0.016	0.008	308	3	22	4.65
XKS-6-2	Stibnite	Level #6, Tongjiayuan, +210	0.6203	5.4	2.73	0.015	0.008	316	4	28	6.73
XKW9	Stibnite	Level #3, Wuhua, unclear	0.1665	1.4	2.64	0.029	0.003	307	8	51	5.73
XKS-23-6	Stibnite	Level #23, Laokuangshan, −120	0.4635	2.3	1.96	0.014	0.002	312	3	37	4.34
XKS-25-3	Stibnite	Level #25, Laokuangshan, −142	0.2550	5.9	2.64	0.012	0.002	314	3	22	7.48
XKS-25-2	Stibnite	Level #25, Laokuangshan, −142	0.4026	6.1	4.75	0.016	0.003	308	3	24	5.46

Notes: $^{40}Ar^*$ is non-atmospheric Ar, $^{40}Ar^* = {}^{40}Ar - [{}^{36}Ar \times 298.6]$. The $^{3}He/Q$ was calculated using the equation $^{3}He/Q = {}^{3}He/{}^{36}Ar \times [{}^{36}Ar]_{masw}/(Cp\theta)$. MASW—modified air-saturated meteoric water.

TABLE 2. CARBON AND OXYGEN ISOTOPE DATA OF THE HYDROTHERMAL CALCITE FROM THE XIKUANGSHAN ANTIMONY DEPOSIT

Stage	Sample	Location and elevation	Mineral assemblage	$\delta^{13}C_{PDB}$ (‰)	$\delta^{18}O_{SMOW}$ (‰)
Early stage	XN3-9	Level #3, Tongjiayuan, +300 m	q + stb + cal	−5.6	18.3
	XN3-10			−6.7	18.4
	XN3-11			−6.0	18.6
	XN3-13			−4.3	17.8
	XN3-15			−8.2	17.8
	XKL-3			−6.6	19.5
Late stage	XS11-5	Level #11, Feishuiyan, +136 m	cal + stb + q	1.9	17.1
	XS11-36*			2.1	17.1
	XS19W-1*	Level #19, Feishuiyan, −34 m		1.9	16.2
	XS19W-3			0.6	16.3
	XS19W-7			1.5	16.0
	XS19W-8			1.9	16.4
	XS19W-13			0.7	16.4
	XS19E-2*			1.5	15.3
	XS19E-1*	Level #19, Feishuiyan, –34 m		1.9	15.0
	XKS-33	Level #11, Tonjiayuan, +136 m		1.0	15.3
	XKS-15	Level #15, Tonjiayuan, +30 m		1.6	15.8
	XKSS-15	Level #21, Feishuiyan, −25 m		0.1	12.7
	XKSS-17			−0.2	12.1
	XKSS-21			1.9	15.7
	XKSS-22			1.5	14.7
	XKSS-24			1.7	14.6
	XKSS-26			0.4	18.0
	XKW-6	Level #3,Wuhua, unclear		0.8	17.1
	XKW-7			1.4	15.9
	XKW-8			0.8	13.8
	XKW-9			0.9	16.1
	XKW-11			−0.1	17.8

Notes: cal—calcite; stb—stibnite; q—quartz; PDB—Peedee belemnite; SMOW—standard mean ocean water.
*Peng and Hu (2001).

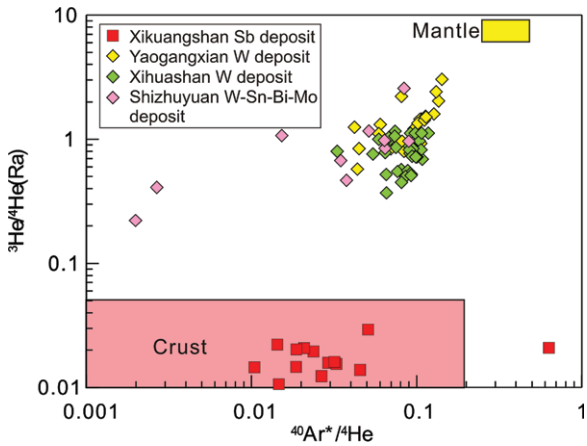

Figure 8. Plots of $^{40}Ar^*/^4He$ versus $^3He/^4He$ of fluid inclusions trapped in stibnites from the Xikuangshan Sb deposit. The ranges of mantle and crustal fluids are defined by the data from Turner et al. (1993), Stuart et al. (1995), Burnard et al. (1999), and Hu et al. (2012). The data of the Yaogangxian W, Xihuashan W, and Shizhuyuan W-Sn-Bi-Mo deposits are, respectively, from Hu et al. (2012), Wei et al. (2019), and Wu et al. (2011).

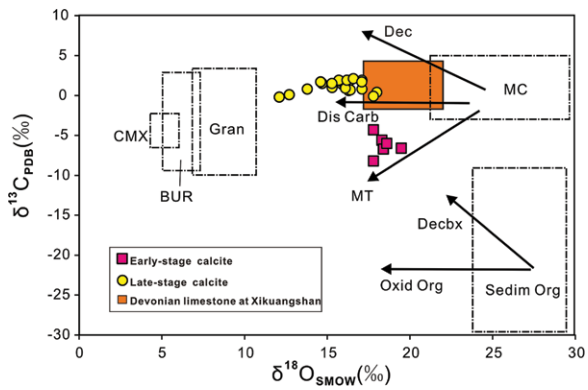

Figure 9. Plots of $\delta^{13}C$ versus $\delta^{18}O$ of the hydrothermal calcites and limestone from the Xikuangshan Sb deposit. For reference, the fields for typical marine carbonates (MC), sedimentary organic matter (Sedim Org), igneous carbonatite and mantle xenoliths (CMX), basic and ultrabasic rocks (BUR), and granite (Gran) are outlined. The arrows show typical isotopic trends resulting from carbonate dissolution (Dis Carb), decarbonation (Dec), decarboxylation of organic matter (Decbx), oxidation of organic matter (Oxid Org), and mixing trend (MT) (modified after Liu et al., 1996, 2003).

of debate. Many workers have suggested that the fluids are magmatic (Wang et al., 1938; Liu et al., 1985), meteoric (Tu, 1984; Liu, 1992; Yang et al., 1998; Hu et al., 2017), marine (Zhang et al., 1998; Liu et al., 2002), or mantle-derived (Li, 1996; Jin et al., 1999). The new integrated isotopic data below, however, indicate that they are modified air-saturated meteoric water (MASW).

Helium-Argon Isotopes

It has been demonstrated that sulfide minerals, including stibnite, are a faithful trap of noble gases in the parental fluids; thus, noble gas loss from the fluid inclusions of the sulfide separates by diffusion is unlikely to be significant for relatively young sulfide minerals (e.g., 160–130 Ma) (Stuart et al., 1994; Jean-Baptiste and Fouquet, 1996; Burnard et al., 1999; Hu et al., 1999; Burnard and Polya, 2004). A primary advantage of crushing samples for analysis of noble gas isotopes is that only a negligible proportion of the lattice-trapped radiogenic He and Ar is likely to be released (Stuart et al., 1994, 1995; Hu et al., 1998a, 1998b, 2012; Burnard et al., 1999). In situ–produced ^4He and ^{40}Ar within the fluid inclusions is also unlikely to be significant even for sulfide minerals from a uranium deposit with an age of ca. 120 Ma (Hu et al., 2009). Cosmogenic production of ^3He can be ruled out here because all of the samples were collected from underground mines (Simmons et al., 1987; Stuart et al., 1995; Burnard et al., 1999). One notable disadvantage of the crushing analytical technique is the difficulty of separating different generations of fluid inclusions that exist in Xikuangshan minerals, and the results thus represent some averaging of different fluid compositions. Fortunately, the fluid inclusions in

TABLE 3. RUBIDIUM AND STRONTIUM ISOTOPE DATA FOR THE ORE-STAGE CALCITE FROM THE XIKUANGSHAN ANTIMONY DEPOSIT

Sample	Rb (ppm)	Sr (ppm)	Rb/Sr	$^{87}Sr/^{86}Sr$ (2σ)
Early stage				
XN3-9	0.37	787.4	0.0005	0.712684 ± 8
XN3-10	1.03	777.0	0.0013	0.712823 ± 7
XN3-11	0.27	814.7	0.0003	0.712193 ± 6
XN3-13	0.72	642.0	0.0011	0.712790 ± 5
XN3-15	0.66	654.5	0.0010	0.712115 ± 7
Late stage				
XS11-5*	8.51	186.8	0.0456	0.712410 ± 8
XS11-36*	0.43	153.5	0.0028	0.710198 ± 8
XS19W-1*	0.65	174.9	0.0037	0.710334 ± 7
XS19W-3	4.17	198.7	0.0210	0.710375 ± 6
XS19W-7	5.57	208.7	0.0267	0.711409 ± 8
XS19W-8	21.0	190.7	0.1101	0.711888 ± 7
XS19W-13	2.63	111.1	0.0237	0.710610 ± 7
XS19E-2*	2.32	147.0	0.0158	0.710317 ± 7
XS19E-1*	1.82	86.8	0.0210	0.710184 ± 6

Notes: From Peng et al. (2001). Locations are shown in Table 2.

TABLE 4. SAMARIUM AND NEODYMIUM ISOTOPE DATA FOR THE HYDROTHERMAL CALCITE FROM THE XIKUANGSHAN ANTIMONY DEPOSIT

Sample	Sm (ppm)	Nd (ppm)	$^{147}Sm/^{144}Nd$	$^{143}Nd/^{144}Nd$ (2σ)	ε_{Nd} (156 Ma)	ε_{Nd} (124 Ma)
Early stage						
XN3-9	0.670	0.251	1.6167	0.513287 ± 24	−15.57	
XN3-10	0.854	0.199	2.5994	0.514287 ± 26	−15.63	
XN3-11	4.43	0.318	8.4197	0.520207 ± 25	−16.03	
XN3-13	0.633	0.407	0.9411	0.512598 ± 22	−15.56	
XN3-15	0.725	0.241	1.8210	0.513495 ± 24	−15.58	
Late stage						
XS11-2	0.373	0.854	0.2643	0.511923 ± 26		−14.97
XS11-5	0.701	0.705	0.6017	0.512198 ± 09		−14.95
XS11-36	0.791	1.56	0.3068	0.511958 ± 24		−14.96
XS19W-1	0.533	3.62	0.0890	0.511782 ± 08		−14.95
XS19W-3	0.914	1.53	0.3616	0.512005 ± 10		−14.94
XS19W-7	1.32	1.95	0.4094	0.512044 ± 18		−14.91
XS19W-13	0.571	0.995	0.3468	0.511988 ± 22		−14.91
XS19E-2	0.402	0.771	0.3154	0.511966 ± 11		−15.01

Notes: Sm and Nd isotopic data are from Peng et al. (2003a). The $^{147}Sm/^{144}Nd$ and $^{143}Nd/^{144}Nd$ of the present-day chondritic uniform reservoir (CHUR) are 0.1967 and 0.512636, respectively. The ages for $\varepsilon_{Nd(t)}$ calibration are from Peng et al. (2003a). Locations are shown in Table 2.

the analyzed stibnite crystals may be dominated by primary ones, because primary fluid inclusions are the dominant types in the associated, transparent minerals based on textural observation (Lin, 2014). Thus, it was concluded that the measured He and Ar isotopes of the volatiles extracted from the stibnite separates from the Xikuangshan Sb deposit (Table 1) could roughly represent the initial isotope compositions of the ore-forming fluids.

Three potential sources for noble gases in fluid in the crust are commonly accepted: air-saturated water, mantle, and radiogenic isotopes produced by decay of U, Th, and K within the crust (Turner et al., 1993; Stuart et al., 1994; Burnard et al., 1999; Hu et al., 2012). Atmospheric He is too low to exert a significant influence on its abundance and isotopic composition in most crustal fluids; thus, He in ore-forming fluids of the deposits have only two possible sources: mantle He and radiogenic He produced within the crust (Turner et al., 1993; Stuart et al., 1994; Hu et al., 2012). The $^{3}He/^{4}He$ ratios of ore-forming fluids for the Xikuangshan deposit ranged from 0.01 to 0.03 Ra, significantly lower than the upper mantle value range of 6–9 Ra, although well within the range of crustal values (0.01–0.05 Ra; Table 1; Turner et al., 1993; Stuart et al., 1994; Burnard et al., 1999; Hu et al., 2004), supporting a crustal origin of He in the fluids.

In the late Mesozoic (160–130 Ma), numerous granite-related W-Sn polymetallic deposits that are generally contemporaneous with the Xikuangshan Sb deposit are present to the eastern end (Hu and Zhou, 2012; Mao et al., 2013; Hu et al., 2017). This raises a possibility of a common source of fluids for these deposits; however, unlike the Xikuangshan Sb deposit (Fig. 8), the ore-forming fluids of the granite-related W-Sn polymetallic deposits that were exsolved from granitic parent magma (e.g., the Yaogangxian, Xihuashan, and Shizhuyuan deposits) contain significant amounts of mantle-derived noble gases in addition to crustal noble gases (Li et al., 2007; Wu et al., 2011; Hu et al., 2012; Wei et al., 2019). This implies that, during the late Mesozoic in or around the Xiangzhong region, there were not "pure" crust-derived S-type granites that could also provide crustal He. Therefore, it was concluded here that the ore-forming fluids of the Xikuangshan Sb deposit are most likely MASW, i.e., air-saturated water (meteoric) with variable additional crustal radiogenic He and Ar (much ^{4}He and little $^{40}Ar^*$, where $^{40}Ar^*$ is non-atmospheric Ar calculated according to the Equation $^{40}Ar^* = {}^{40}Ar - [{}^{36}Ar \times 298.6]$).

The $^{40}Ar^*/^{4}He$ of the Xikuangshan deposit ranged from 0.01 to 0.05 (average, 0.03; excluding one outlier sample, 0.64; Table 1 and Fig. 8), significantly lower than the average crustal ratio (~0.2; Torgersen et al., 1989; Ballentine and Burnard, 2002), and thus suggesting preferential acquirement of ^{4}He relative to ^{40}Ar from the crustal rocks via the fluid pathway. Modern groundwater commonly has a much lower $^{40}Ar^*/^{4}He$ value than the crustal ratio, likely the result of preferential ^{4}He acquirement relative to ^{40}Ar from the crust due to higher closure temperature of the latter Ar (Torgersen et al., 1989; Ballentine and Burnard, 2002; Hu et al., 2012). For the majority of minerals, the closure temperature of He is commonly <200 °C, whereas Ar is quantitatively retained in most minerals at 250 °C (Lippolt and Weigel, 1988; McDougall and Harrison, 1988; Elliot et al., 1993). Based on fluid inclusion thermometry of coexisting quartz and calcite, the mineralization temperature of the Xikuangshan deposit is 140–250 °C (Lin, 2014). At these temperatures, the fluids would have gained much more He than Ar from the crustal rocks; therefore, it was concluded here that the ore-forming fluids of the Xikuangshan Sb deposit are initially of low-temperature, meteoric groundwater origin. Further, the noble gases in the fluids were derived from two major reservoirs: most Ar from the initial air-saturated meteoric water and most He from the crustal rocks in the pathway of the fluid, resulting from water-rock interaction.

Additionally, the ^{4}He concentrations of the early-stage stibnite (9.9×10^{-7}–97.5×10^{-7} cm^3 STP g^{-1} (average, 25.2×10^{-7} cm^3 STP g^{-1}) are five times higher than those of the late-stage stibnite (1.4×10^{-7}–6.1×10^{-7} cm^3 STP g^{-1} (average, 4.7×10^{-7} cm^3 STP g^{-1}), suggesting more ^{4}He was extracted out from crustal rocks by the ore-forming fluids responsible for the early-stage stibnite (Table 1). This could arise from either the higher temperature of the early-stage fluids, or most likely from the greater intensity of water-rock interactions during this stage, the latter of which can be further verified by the co-variation relationship of Sr-O isotopes of calcites deposited in these two stages (discussed in further detail in the next section).

Carbon-Oxygen-Strontium Isotopes

The C and O isotopes of hydrothermal calcites and limestone host rocks of the Xikuangshan Sb deposit are compared with other rocks and reservoir types (Liu and Liu, 1997; Liu et al., 2003) in Figure 9. The "fresh" host carbonate rocks have similar $\delta^{13}C$ values and lower $\delta^{18}O$ values than those of typical marine limestones. The C-O isotopic decoupling is consistent with interaction of meteoric hydrothermal fluids. Compared to Devonian limestones, the early-stage calcites of the deposit had lower $\delta^{13}C$ values, and the late-stage calcites of the deposit had overall lower $\delta^{18}O$ values. A plausible interpretation for such variations is that the CO_2 in the ore-forming fluids of both stages was derived primarily from marine limestones in the pathway by dissolution (Fig. 9); however, a significant amount of CO_2 in the early-stage ore-forming fluids could also be organic carbon from country rocks by oxidation and/or decarboxylation reaction during water-rock interaction. A more significant magmatic input could also explain the lower $\delta^{13}C$ values, although direct evidence for this is lacking.

Based on the isotope fractionation equation between calcite and water ($1000\ln\alpha_{calcite\text{-}water} = 2.78 \times 10^6/T^2 - 3.39$; O'Neil et al., 1969), the calculated $\delta^{18}O_{H2O}$ values of the early- and late-stage ore-forming fluids of the Xikuangshan deposit are from +5.8‰ to +7.6‰ and from +0.5‰ to –9.3‰, respectively, markedly higher than estimated values for the Mesozoic meteoric water in the region (~–10‰, Zhang, 1989). The

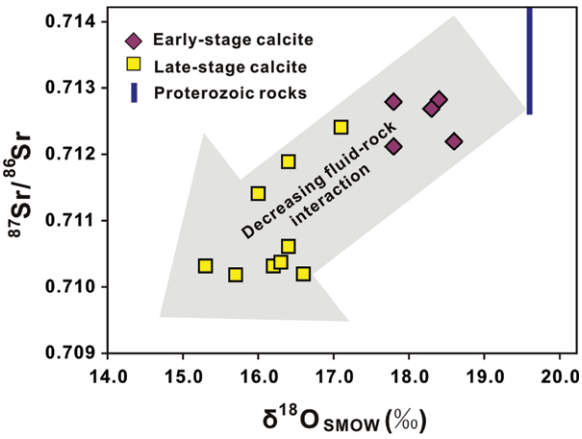

Figure 10. Plots of $\delta^{18}O$ versus $^{87}Sr/^{86}Sr$ of the hydrothermal calcites from the Xikuangshan Sb deposit. The $^{87}Sr/^{86}Sr$ and average $\delta^{18}O$ values of the Proterozoic metamorphic rocks are, respectively, from Peng et al. (2001) and Ma et al. (2003). SMOW—standard mean ocean water.

difference could be due to the addition of magmatic fluid (+5.5‰ to +8.5‰; Ohmoto, 1986) to the ore-forming fluids or a highly evolved meteoric water for the fluids. The strong positive correlation between $\delta^{18}O$ and $^{87}Sr/^{86}Sr$ for the ore-stage calcites of the deposit is more consistent with the latter interpretation (Fig. 10). It was verified that $\delta^{18}O$ and $^{87}Sr/^{86}Sr$ of meteoric hydrothermal fluids would become rock-buffered through water-rock interaction until equilibrium (Barker et al., 2009; Satish-Kumar et al., 2010; Beaudoin and Chiaradia, 2016). Between the two stages of hydrothermal calcites of the deposit, the early-stage calcites have significantly greater $\delta^{18}O$ and $^{87}Sr/^{86}Sr$ values, possibly resulting from the higher intensity of water-rock interactions compared to the late-stage ones. Accordingly, the early-stage ore-forming fluids acquired more amounts of ^{18}O and ^{87}Sr from the crustal rocks that are enriched in both $\delta^{18}O$ and $^{87}Sr/^{86}Sr$ values. The Neoproterozoic rocks in the region have such high isotopic compositions (Fig. 10; Peng et al., 2001; Ma et al., 2003). Further, analogous interpretations have been proposed to explain the origin of hydrothermal minerals with elevated $\delta^{18}O$ and $^{87}Sr/^{86}Sr$ values elsewhere in the world (Savard and Kontak, 1998; Barker et al., 2009; Satish-Kumar et al., 2010; Beaudoin and Chiaradia, 2016).

It is important to note that there is an inverse relationship between measured $^{87}Sr/^{86}Sr$ and Rb/Sr ratios of the hydrothermal calcites from the Xikuangshan Sb deposit. Accordingly, the early-stage calcites have higher measured $^{87}Sr/^{86}Sr$ and lower Rb/Sr ration than the late-stage calcites (Table 3). The inverse relationship indicates that the contrasting measured $^{87}Sr/^{86}Sr$ ratios between these two different stages of calcites are likely not due to the radiogenic growth of ^{87}Sr from ^{87}Rb in the samples. For this reason, the Rb/Sr in the calcites can be used as an independent genetic indicator. Thus, it is suggested here that such variation derived from different degrees of water-rock interaction, with a higher intensity of water-rock interaction for the early stage. Further, it is envisioned here that a larger amount of Sr was released from the crustal rocks with increasing intensity of water-rock interaction. This is also consistent with the significantly higher ^{4}He concentration for early- versus late-stage stibnite (as described above). Therefore, it is proposed that as the intensity of water-rock interaction increases, more Sb was released from the rocks to the fluids, consistent with the dominant amount of Sb (>80% of the total Sb reserve) deposited in the early-stage versus the late-stage mineralization (Wen et al., 1993; Hu and Peng, 2018).

Notably, the early-stage versus late-stage average enrichment times of the concentrations for calcite Sr (735/162 = 4.5) (Table 3) and stibnite ^{4}He (25.2/4.7 = 5.4) (Table 1), as well as the Sb reserves (>80/20 > 4), are nearly equal, possibly representing the intensity index of the water-rock interactions at the early and late stages.

Sources of Antimony

Although the Xikuangshan deposit has been the focus of numerous previous studies, the precise source of the Sb remains unclear. To date, different origins have been proposed including Devonian host rocks (Tu, 1984; Xiao and Li, 1984; Zou, 1988; Wen et al., 1993; Fan et al., 2004), marine rocks (Zhang et al., 1998; Liu et al., 2002), intrusive rocks at depth (Liu et al., 1985; Lin et al., 1987; Li, 1993), and the Neoproterozoic rocks in the basement of the Xiangzhong basin (e.g., Peng et al., 2001, 2002; Ma et al., 2002, 2003). Based on Sr-Nd isotope data and the concentrations of Sb in different types of rocks in the region, it is concluded here that most of Sb in the Xikuangshan deposit was derived from the basement rocks of the basin, as discussed in more detail below.

Strontium-Neodymium Isotopes

Strontium isotope fractionation between calcite and a hydrothermal fluid is insignificant (Kontak and Jackson, 1997; Savard and Kontak, 1998). Further, the Rb/Sr ratios of the ore-stage calcites of the Xikuangshan deposit are very low (Table 3). As a result, the amounts of ^{87}Sr in the calcites produced by decay of ^{87}Rb to ^{87}Sr are negligible, and the measured $^{87}Sr/^{86}Sr$ ratios of ore-stage calcites from this deposit approximate the initial ratios of the parental fluids for the deposit. The $^{87}Sr/^{86}Sr$ ratios of the ore-forming fluids of the deposit, as inferred from the values of the early- and late-stage calcites (0.7102–0.7128, Table 3), were much higher than those of circulating hydrothermal fluids in modern oceanic ridges (0.7035 ± 5; Albarède et al., 1981; Piepgras and Wasserburg, 1985), present-day seawater (0.709241 ± 32; Elderfield, 1986), and Phanerozoic seawater (0.7067–0.7092; Veizer, 1989), thereby excluding seawater or heated, circulating seawater as the ore-forming fluids of the Xikuangshan Sb deposit.

Owing to the relatively homogeneous Sr isotopic composition of seawater, and the lack of significant fractionation of Sr isotopes during carbonate precipitation from seawater (Veizer, 1989), marine carbonate and seawater are expected to have similar $^{87}Sr/^{86}Sr$ ratios. The host Devonian marine limestones of the Xikuangshan deposit maintained $^{87}Sr/^{86}Sr$ ratios of 0.7078–0.7086 (Lu et al., 1994), markedly similar to those of seawater, but lower than those of the ore-forming fluids inferred from the hydrothermal calcites of the Xikuangshan deposit (0.7102–0.7128; Table 3). Such inverse relationship indicates that the elevated $^{87}Sr/^{86}Sr$ ratios of the ore-forming fluids were not the result of in situ exchange reaction with the immediate Devonian country rocks at Xikuangshan but were rather acquired at depth from the rocks that have high $^{87}Sr/^{86}Sr$ ratios, such as the Mesozoic granites ($^{87}Sr/^{86}Sr$ = 0.705–0.730; Chen and Jahn, 1998) and Proterozoic rocks ($^{87}Sr/^{86}Sr$ 0.713–0.726; Peng et al., 2001) found in the region. Among these two alternatives, the latter is a better choice after considering Sm-Nd isotope data as well. The $\varepsilon_{Nd}(t)$ values of the Mesozoic granites (−10.15 to −11.91; Fu, 2015) were much higher than those of the hydrothermal calcites of the Xikuangshan deposit (−16.03 to −14.95; Table 4); whereas in contrast, the $\varepsilon_{Nd}(t)$ values of the Neoproterozoic rocks at the time of mineralization (Li, 1996; Mao et al., 1997; Zhu, 1997) are from −10.3 to −15.2, similar to the ore-stage calcite $\varepsilon_{Nd}(t)$ values of the Xikuangshan deposit (Table 4).

Antimony Abundances

The Devonian carbonate host rocks of the Xikuangshan deposit are unlikely to be the

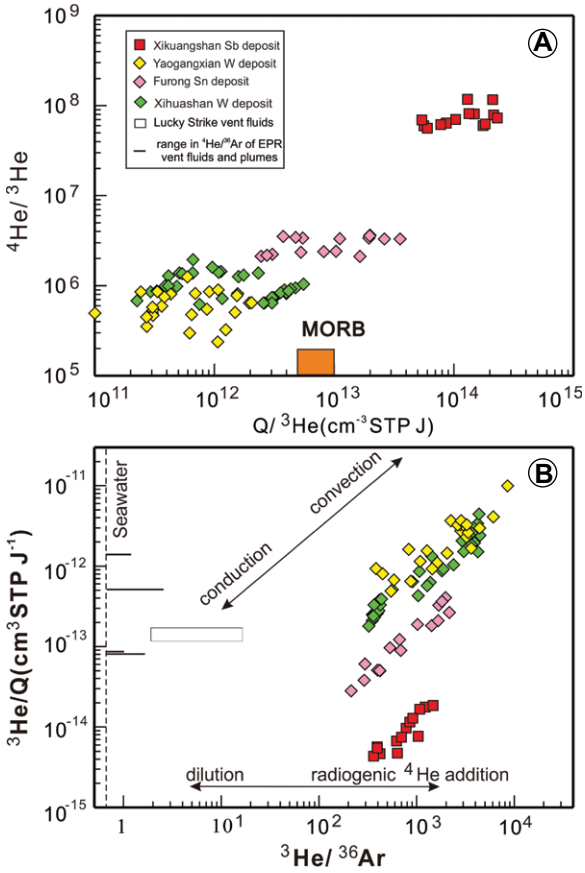

Figure 11. Plots of (A) Q/^{3}He versus ^{4}He/^{3}He and (B) ^{4}He/^{36}Ar versus ^{3}He/Q of the inclusion fluids trapped by stibnites from the Xikuangshan Sb deposit (modified after Burnard and Polya, 2004). The ranges of Lucky Strike vent fluids and East Pacific Rise (EPR) vent fluids are defined by the data from Jean-Baptiste et al. (1998), Lupton et al. (1989), and Lupton et al. (1995). The plots of the Yaogangxian W, Xihuashan W, and Shizhuyuan W-Sn-Bi-Mo deposits are calculated, respectively, from the raw data of Hu et al. (2012), Wei et al. (2019), and Wu et al. (2011). MORB—mid-oceanic ridge basalt; STP—standard temperature and pressure.

major source of Sb for the deposit, because they maintain very low Sb contents (0.4–0.8 ppm; Xie, 1996; Lu et al., 2001). Though the shales in the Devonian were thought to be source beds because of their relatively elevated Sb contents (Fan et al., 2004), in spite of their limited thickness, the abnormally elevated Sb contents determined by semiquantitative spectrochemical analyses most likely arose from their either low analytical precisions or sampling localities near mineralization (Yang et al., 2006). Furthermore, the least altered host rocks of the Xikuangshan deposit generally contain much lower Sb (average, 0.9 ppm) than the severely altered host rocks (up to 46 ppm; Ma et al., 2002), thereby ruling out the potential of in situ extraction of Sb from the country rocks during alteration (Ma et al., 2003; Hu et al., 2017). The Mesozoic granitic rocks in the region are also unlikely to be the source of Sb for the deposit, because their Sb concentrations are also very low (0.26–0.74 ppm; Shi et al., 1993; Jin et al., 1999).

Alternatively, the Proterozoic rocks in the basement of the basin are most likely the Sb source for the deposit, as these rocks have the highest Sb abundances in the studied region (7.8–27.2 ppm; Ma, 1999; Lu et al., 2001; Ma et al., 2002). Hydrothermal leaching experiments indicate that 20%–90% of Sb can be transferred from this type of rock to fluids at 200 °C (Niu and Ma, 1991; He and Ma, 1996; Ma et al., 2002). More recently, an antimony isotope study suggests that the Neoproterozoic basements might have served as the primary metal source for this deposit (Zhai et al., 2021). The presence of many Sb deposits that were directly hosted in the Proterozoic strata, including several relatively large ones such as the Woxi, Banxi, Fuzhuxi, and Zhazixi deposits (Fig. 1B), further supports the interpretation here that the Proterozoic rocks are the main source of Sb for the Xikuangshan deposit.

Heat Source

Heat is essential for the production and circulation of hydrothermal fluids. Generally, heat and ^{4}He in the earth are both produced by the decay of U and Th; whereas the observed helium/heat (^{3}He/Q) ratios in crustal fluids may carry useful information on the transporting mechanisms of heat, and volatiles within the earth (Turner and Stuart, 1992). Because the conductive transfer of heat without volatiles into a system will fractionate ^{3}He from heat (Burnard and Polya, 2004), heat fluxes transported to the crust by conduction would have much lower ^{3}He/Q ratios than that transported by convection (Castro et al., 2005, 2007). Hence, the ^{3}He/Q ratios are often used to constrain the mechanism of heat transfer. The ^{3}He/Q ratio can be obtained by the equation $^3\mathrm{He/Q} = {}^3\mathrm{He}/{}^{36}\mathrm{Ar} \times [{}^{36}\mathrm{Ar}]_{masw}/(C_p\theta)$, where $[{}^{36}\mathrm{Ar}]_{masw}$ is the concentration of ^{36}Ar in modified air-saturated water, *Cp* is the specific heat of MASW, and θ is the temperature increase of the cold fluid (Burnard et al., 1999; Burnard and Polya, 2004). The estimated ^{3}He/Q ratios of the ore-forming fluids at Xikuangshan are from 4.3 to 18.5 × 10^{-15} cm^3 STP J^{-1} (Fig. 11; Table 1), notably three orders of magnitude lower than those recorded by the hydrothermal fluids of the mid-oceanic ridge vents (0.1 − 1.0 × 10^{-12} cm^3 STP J^{-1}; Lupton et al., 1989; Baker and Lupton, 1990), and of the Mesozoic granite-related W-Sn polymetallic deposits, such as the contemporaneous Yaogangxian W, Xihuashan W, and Shizhuyuan W-Sn-Bi-Mo deposits in the neighboring regions (Fig. 11). The ore-forming fluids of the three coeval W-Sn polymetallic deposits were demonstrated to be exsolved from the related granitic magma (Li et al., 2007; Wu et al., 2011; Hu et al., 2012; Wei et al., 2019); thus heat was likely acquired by convection from this source (Fig. 11). Therefore, the significantly lower ^{3}He/Q values suggest that the deep-seated magma could have provided heat by conduction without transferring volatiles to the ore-forming fluids of the Xikuangshan Sb deposit.

Granitic xenoliths in the postmineralization lamprophyre dike within the deposit and geophysical data show that there are buried granites beneath the Xikuangshan deposit (Rao et al., 1999; Wu and Hu, 2000). Since late Mesozoic (Yanshanian) granites are regionally common (Hu and Zhou, 2012; Mao et al., 2013), the inferred granites beneath this deposit could be of late Mesozoic ages, contemporaneous with the ore formation of the deposit. As discussed above, there was no evidence of magmatic chemical components in the ore-forming fluids of the deposit. This suggests that the granitic magma beneath the Xikuangshan ore-forming system provided only conductive heat to this system, notably consistent with the geothermal genetic model for the Xikuangshan Sb deposit (Yang et al., 2003).

A Comprehensive Genetic Model

The stratabound model, proposed by Xiao and Li (1984), can reasonably explain the occurrence of stratiform-like orebodies but cannot account for the source of Sb, as the Devonian limestone host strata are extremely Sb poor. Similarly, the syn-genetic seafloor exhalation model of Zhang et al. (1998) and Liu et al. (2002) and the sed-

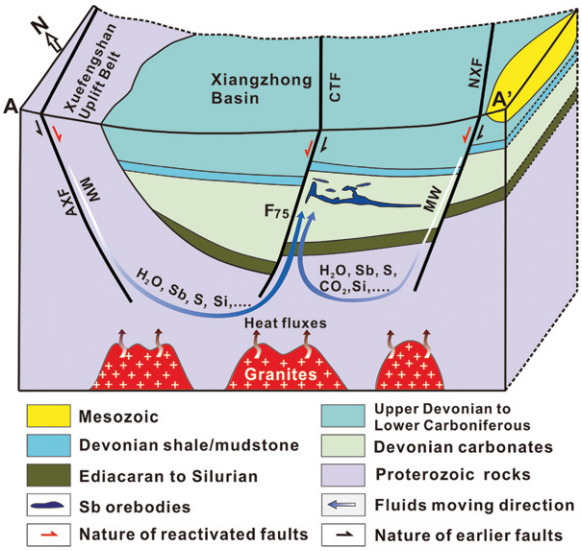

Figure 12. A schematic diagram for the genetic model of the Xikuangshan Sb deposit. AXF—Anhua-Xupu fault; CTF—Chengbu-Taojiang fault; MW—meteoric water; NXF—Ningxiang-Xinning fault.

imentary-diagenetic model of Fan et al. (2004) are inconsistent with the deposit formation age between Jurassic and Early Cretaceous (160–130 Ma), more than 200 m.y. after the formation of the Devonian host rocks. Accordingly, a new comprehensive genetic model has been proposed here that can adequately explain the geological and isotopic data of this deposit (Fig. 12):

(1) The late Mesozoic (Yanshanian) tectonic event resulted in the formation of a giant Yanshanian granite province (swath >1000 km wide) across the whole Cathaysian and eastern Yangtze Blocks, with the peak ages of 160–140 Ma. The Xikuangshan Sb deposit in the eastern Yangtze Block and numerous granite-related W-Sn polymetallic deposits in the Cathaysia Block, to the east of the Xikuangshan, formed during this period.

(2) Among the different lithologies in the Xiangzhong basin, where the Xikuangshan and surrounding regions are located, the Neoproterozoic rocks have the highest Sb contents, and thus served as the primary Sb source in the Xikuangshan deposit.

(3) The deep-seated Yanshanian granitic magma in the region had provided heat in the way of conduction to the cover rocks, heating the meteoric groundwater and triggering large-scale circulation of these fluids. The heated fluids extensively interacted with the underlying Sb-rich Neoproterozoic low-grade metamorphic rocks, extracted Sb, and other components (e.g., S) to derive the ore-forming fluids of the Xikuangshan Sb deposit.

(4) The ore-forming fluids ascended through the regional fault F_{75} and subsequently deposited Sb as stibnites at favorable structural traps, ultimately forming the giant Xikuangshan Sb deposit.

CONCLUSIONS

(1) The ore-forming fluid of the Xikuangshan Sb deposit is a kind of modified air-saturated meteoric water that had gained Sb and other components predominantly from the underlying Sb-rich Neoproterozoic low-grade metamorphic rocks through extensive water-rock interaction although CO_2 mainly from dissolution of marine carbonate strata.

(2) The deep-seated granitic magma had provided heat by conduction to the overlying ore-forming systems. The heated meteoric groundwater circulated in, interacted with, and extracted out of Sb from the Sb-rich Neoproterozoic rocks to form ore-forming fluids. The ore-forming fluids used the major fault F_{75} as a conduit and deposited Sb as stibnites at Xikuangshan to form such giant Sb deposit.

(3) The occurrence of Sb-rich source rocks at depth, as well as extensive interaction between these rocks and heated meteoric groundwater are two of the most important constraints on the formation of the giant Xikuangshan Sb deposit. Due to much more extensive water-rock interaction relative to the late stage, the early-stage mineralization produced >80% of the Sb reserves of the deposit.

ACKNOWLEDGMENTS

This work was jointly funded by the National Natural Science Foundation of China (41830432, U1812402, 41703044), the National Key R&D Program of China (2018YFC0603505), and the Field Forefront Project of the State Key Laboratory of Ore Deposit Geochemistry, Institute of Geochemistry, Chinese Academy of Sciences (202102). We thank Dr. Chusi Li from Indiana University, USA, for his constructive comments and suggestions on the earlier manuscript, and the geologists of the Xikuangshan Mine for their help during our field work.

REFERENCES CITED

Albarède, F., Michard, A., Minster, J.F., and Michard, G., 1981, $^{87}Sr/^{86}Sr$ ratios in hydrothermal waters and deposits from the East Pacific Rise at 21°N: Earth and Planetary Science Letters, v. 55, p. 229–236, https://doi.org/10.1016/0012-821X(81)90102-3.

Baker, E.T., and Lupton, J.E., 1990, Changes in submarine hydrothermal ^{3}He/heat ratios as an indicator of magmatic/tectonic activity: Nature, v. 346, p. 556–558, https://doi.org/10.1038/346556a0.

Ballentine, C.J., and Burnard, P.G., 2002, Production, release and transport of noble gases in the continental crust: Reviews in Mineralogy and Geochemistry, v. 47, p. 481–538, https://doi.org/10.2138/rmg.2002.47.12.

Barker, S.L.L., Bennett, V.C., Cox, S.F., Norman, M.D., and Gagan, M.K., 2009, Sm–Nd, Sr, C and O isotope systematics in hydrothermal calcite-fluorite veins: Implications for fluid-rock reaction and geochronology: Chemical Geology, v. 268, p. 58–66, https://doi.org/10.1016/j.chemgeo.2009.07.009.

Beaudoin, G., and Chiaradia, M., 2016, Fluid mixing in orogenic gold deposits: Evidence from the H-O-Sr isotope composition of the Val-d'Or vein field (Abitibi, Canada): Chemical Geology, v. 437, p. 7–18, https://doi.org/10.1016/j.chemgeo.2016.05.009.

Burnard, P.G., and Polya, D.A., 2004, Importance of mantle-derived fluids during granite associated hydrothermal circulation: He and Ar isotopes of ore minerals from Panasqueira: Geochimica et Cosmochimica Acta, v. 68, p. 1607–1615, https://doi.org/10.1016/j.gca.2003.10.008.

Burnard, P.G., Hu, R.Z., Turner, G., and Bi, X.W., 1999, Mantle, crustal and atmospheric noble gases in Ailaoshan Gold deposits, Yunnan Province, China: Geochimica et Cosmochimica Acta, v. 63, p. 1595–1604, https://doi.org/10.1016/S0016-7037(99)00108-8.

Castro, M.C., Patriarche, D., and Goblet, P., 2005, 2-D numerical simulations of groundwater flow, heat transfer and ^{4}He transport—Implications for the He terrestrial budget and the mantle helium-heat imbalance: Earth and Planetary Science Letters, v. 237, p. 893–910, https://doi.org/10.1016/j.epsl.2005.06.037.

Castro, M.C., Patriarche, D., Goblet, P., Ma, L., and Hall, C.M., 2007, ^{4}He/Heat Flux Ratios as New Indicators of Past Thermal and Tectonic Events—New Constraints on the Tectonothermal History of the Michigan Basin: Potsdam, Germany, Proceedings of the 4th Mini Conference on Noble Gases in the Hydrosphere and in Natural Gas Reservoirs 28 February 2007 to 2 March 2007.

Charvet, J., 2013, The Neoproterozoic–Early Paleozoic tectonic evolution of the South China Block: an overview: Journal of Asian Earth Sciences, v. 74, p. 198–209, https://doi.org/10.1016/j.jseaes.2013.02.015.

Chen, J.F., and Jahn, B.M., 1998, Crustal evolution of southeastern China: Nd and Sr isotopic evidence: Tectonophysics, v. 284, p. 101–133, https://doi.org/10.1016/S0040-1951(97)00186-8.

Chen, W.F., Chen, P.R., Huang, H.Y., Ding, X., and Sun, T., 2007, Chronological and geochemical studies of granite and enclave in Baimashan pluton, Hunan, South China: Science in China. Series D, Earth Sciences, v. 50, p. 1606–1627, https://doi.org/10.1007/s11430-007-0073-1.

Chu, Y., Faure, M., Lin, W., Wang, Q.C., and Ji, W.B., 2012a, Tectonics of the Middle Triassic intracontinental Xuefengshan Belt, South China: New insights from structural and chronological constraints on the basal decollement zone: International Journal of Earth Sciences, v. 101, p. 2125–2150, https://doi.org/10.1007/s00531-012-0780-5.

Chu, Y., Lin, W., Faure, M., Wang, Q.C., and Ji, W.B., 2012b, Phanerozoic tectonothermal events of the Xuefengshan Belt, central South China: Implications from U-Pb age and Lu-Hf determinations of granites: Lithos, v. 150, p. 243–255, https://doi.org/10.1016/j.lithos.2012.04.005.

Davidheiser-Kroll, B., Stuart, F.M., and Boyce, A.J., 2014, Mantle heat drives hydrothermal fluids responsible for carbonate-hosted base metal deposits: Evidence from $^{3}He/^{4}He$ of ore fluids in the Irish Pb-Zn ore district:

Mineralium Deposita, v. 49, p. 547–553, https://doi.org/10.1007/s00126-014-0516-5.

Ding, X., Chen, P.R., Chen, W.F., Huang, H.Y., and Zhou, X.M., 2006, Single zircon LA-ICPMS U-Pb dating of Weishan granite (Hunan, South China) and its petrogenetic significance: Science in China. Series D, Earth Sciences, v. 49, p. 816–827, https://doi.org/10.1007/s11430-006-0816-4.

Elderfield, H., 1986, Strontium isotope stratigraphy: Palaeogeography, Palaeoclimatology, Palaeoecology, v. 57, p. 71–90, https://doi.org/10.1016/0031-0182(86)90007-6.

Elliot, T., Ballentine, C.J., O'Nions, R.K., and Ricchiuto, T., 1993, Carbon, helium, neon and argon isotopes in a Po basin natural gas field: Chemical Geology, v. 106, p. 429–440, https://doi.org/10.1016/0009-2541(93)90042-H.

Fan, D.L., Zhang, T., and Ye, J., 2004, The Xikuangshan Sb deposit hosted by the Upper Devonian black shale series, Hunan, China: Ore Geology Reviews, v. 24, p. 121–133, https://doi.org/10.1016/j.oregeorev.2003.08.005.

Faure, M., Shu, L.S., Wang, B., Charvet, J., Choulet, F., and Monie, P., 2009, Intracontinental subduction: A possible mechanism for the Early Palaeozoic Orogen of SE China: Terra (Helsinki, Finland), v. 21, p. 360–368, https://doi.org/10.1111/j.1365-3121.2009.00888.x.

Fu, S.L., 2015, Petrogenesis and chronology of Indosinian granites and the genetic links to the Sb-Au mineralization in central Hunan [Ph.D. thesis]: Beijing, University of Chinese Academy of Sciences, p. 1–166 [in Chinese with English abstract].

Fu, S.L., Hu, R.Z., Bi, X.W., Chen, Y.W., Yang, J.H., and Huang, Y., 2015, Origin of Triassic granites in central Hunan Province, South China: Constraints from zircon U-Pb ages and Hf and O isotopes: International Geology Review, v. 57, p. 97–111, https://doi.org/10.1080/00206814.2014.996258.

Fu, S.L., Hu, R.Z., Chen, Y.W., and Luo, J.C., 2016, Chronology of the Longshan Au- Sb deposit in central Hunan Province: Constraints from pyrite Re-Os and zircon U-Th/He isotopic dating [in Chinese with English abstract]: Yanshi Xuebao, v. 32, p. 3507–3517.

Fu, S.L., Hu, R.Z., Yan, J., Lan, Q., and Gao, W., 2019, The mineralization age of the Banxi Sb deposit in Xiangzhong metallogenic province in southern China: Ore Geology Reviews, v. 112, p. 103033, https://doi.org/10.1016/j.oregeorev.2019.103033.

Fu, S.L., Hu, R.Z., Batt, G.E., Danisik, M., Evans, N.J., and Mi, X.F., 2020, Zircon (U-Th)/He thermochronometric constraints on the mineralization of the giant Xikuangshan Sb deposit in central Hunan, South China: Mineralium Deposita, v. 55, p. 901–912, https://doi.org/10.1007/s00126-019-00906-3.

HBGMR (Hunan Bureau of Geology & Mineral Resources), 1988, Regional Geology of Hunan Province, China: Beijing, Geological Publishing House, p. 718 (in Chinese with English summary).

He, J., and Ma, D.S., 1996, Leaching experiment of gold, antimony, mercury and arsenic from the strata under epithermal-mesothermal conditions in sulfur- and chlorine-bearing solutions [in Chinese with English abstract]: Dizhi Lunping, v. 42, p. 76–85.

Hoefs, J., 1987, Stable Isotope Geochemistry (3rd edition): Berlin, Heidelberg, Springer-Verlag, 241 p., https://doi.org/10.1007/978-3-662-09998-8.

Hu, A.X., and Peng, J.T., 2018, Fluid inclusions and ore precipitation mechanism in the giant Xikuangshan mesothermal antimony deposit, South China: Conventional and infrared microthermometric constraints: Ore Geology Reviews, v. 93, p. 49–56.

Hu, R.Z., 2021, Large scale low-temperature metallogenesis in South China: Beijing, Science Press, p. 314–329 [in Chinese].

Hu, R.Z., and Zhou, M.F., 2012, Multiple Mesozoic mineralization events in South China—An introduction to the thematic issue: Mineralium Deposita, v. 47, p. 579–588, https://doi.org/10.1007/s00126-012-0431-6.

Hu, R.Z., Burnard, P.G., Turner, G., and Bi, X.W., 1998a, Helium and Argon isotope systematics in fluid inclusions of Machangqing copper deposit in west Yunnan province, China: Chemical Geology, v. 146, p. 55–63, https://doi.org/10.1016/S0009-2541(98)00003-5.

Hu, R.Z., Turner, G., Burnard, P.G., Zhong, H., Ye, Z.J., and Bi, X.W., 1998b, Helium and argon isotopic geochemistry of Jinding superlarge Pb-Zn deposit: Science in China. Series D, Earth Sciences, v. 41, p. 442–448, https://doi.org/10.1007/BF02932698.

Hu, R.Z., Bi, X.W., Turner, G., and Burnard, P.G., 1999, He and Ar isotopic geochemistry of the ore-forming fluids of the Ailaoshan Au ore belt [in Chinese]: Science in China. Series D, Earth Sciences, v. 29, p. 321–330.

Hu, R.Z., Burnard, P.G., Bi, X.W., Zhou, M.F., Peng, J.T., Su, W.C., and Wu, K.X., 2004, Helium and argon isotope geochemistry of alkaline intrusion-associated gold and copper deposits along the Red River-Jinshajiang fault belt, SW China: Chemical Geology, v. 203, p. 305–317, https://doi.org/10.1016/j.chemgeo.2003.10.006.

Hu, R.Z., Burnard, P.G., Bi, X.W., Zhou, M.F., Peng, J.T., Su, W.C., and Zhao, J.H., 2009, Mantle-derived gaseous components in ore-forming fluids of the Xiangshan uranium deposit, Jiangxi province, China: Evidence from He, Ar and C isotopes: Chemical Geology, v. 266, p. 86–95, https://doi.org/10.1016/j.chemgeo.2008.07.017.

Hu, R.Z., Bi, X.W., Jiang, G.H., Chen, H.W., Peng, J.T., Qi, Y.Q., Wu, L.Y., and Wei, W.F., 2012, Mantle-derived noble gases in ore-forming fluids of the granite-related Yaogangxian tungsten deposit, Southeastern China: Mineralium Deposita, v. 47, p. 623–632, https://doi.org/10.1007/s00126-011-0396-x.

Hu, R.Z., Fu, S.L., Huang, Y., Zhou, M.F., Zhao, C.H., Wang, Y.J., Bi, X.W., and Xiao, J.F., 2017, The giant South China Mesozoic low-temperature metallogenic domain: Reviews and a new geodynamic model: Journal of Asian Earth Sciences, v. 137, p. 9–34, https://doi.org/10.1016/j.jseaes.2016.10.016.

Jaguin, J., Boulvais, P., Boiron, M.C., Poujol, M., Gapais, D., Ruffet, G., and Briant, N., 2014, Stable isotopes (O, C) and fluid inclusion study of quartz-carbonate veins from the antimony line, Murchison greenstone belt: American Journal of Science, v. 314, p. 1140–1170, https://doi.org/10.2475/07.2014.03.

Jahn, B.M., Bernard-Griffiths, J., Charlot, R., Cornichet, J., and Vidal, F., 1980, Nd and Sr isotopic compositions and REE abundances of cretaceous MORB (Holes 417D and 418A, Legs 51, 52 and 53): Earth and Planetary Science Letters, v. 48, p. 171–184, https://doi.org/10.1016/0012-821X(80)90180-6.

Jean-Baptiste, P., and Fouquet, Y., 1996, Abundance and isotopic composition of helium in hydrothermal sulfides from the East Pacific Rise at 13°N: Geochimica et Cosmochimica Acta, v. 60, p. 87–93, https://doi.org/10.1016/0016-7037(95)00357-6.

Jean-Baptiste, P., Bougault, H., Vangriesheim, A., Charlou, J.L., Raford-Knoery, J., Fouquet, Y., Needham, D., and German, C., 1998, Mantle ^{3}He in hydrothermal vents and plume of the Lucky Strike site (MAR 37°17′) and associated geothermal heat flux: Earth and Planetary Science Letters, v. 157, no. 1–2, p. 69–77, https://doi.org/10.1016/S0012-821X(98)00022-3.

Jin, J.F., Tao, Y., Lai, W.C., and Zeng, L.J., 1999, Metallogenic regularities and direction for prospecting of Xikuangshan-type antimony deposits in central part of Hunan Province: China. Chendu, Sichuan Publishing House of Science & Technology, p. 75–82 (in Chinese).

Jin, J.F., Tao, Y., and Zeng, L.J., 2001, The ore-forming fluid of Xikuangshan-type antimony deposits: Bulletin of Mineralogy [in Chinese with English abstract]: Petrology and Geochemistry, v. 3, p. 156–164.

Johnson, J.P., and McCulloch, M.T., 1995, Sources of ore fluids for the Olympic Dam deposit (South Australia): Sm-Nd isotopic constraints: Chemical Geology, v. 121, p. 177–199, https://doi.org/10.1016/0009-2541(94)00125-R.

Kontak, D.J., and Kerrich, R., 1997, An isotopic (C, O, Sr) study of vein gold deposits in the Meguma Terrane, Nova Scotia; implication for source reservoirs: Economic Geology, v. 92, p. 161–180, https://doi.org/10.2113/gsecongeo.92.2.161.

Kuang, W.L., 2000, Research on the metallogenic model of Xikuangshan superlarge antimony deposit [in Chinese with English abstract]: World Geology, v. 19, p. 26–30.

Lepvrier, C., Maluski, H., Vu, V.T., Leyreloup, A., Phan, T.T., and Nguyen, V.V., 2004, The Early Triassic Indosinian Orogeny in Vietnam (Truong Son Belt and Kontum Massif): Implications for the geodynamic evolution of Indochina: Tectonophysics, v. 393, p. 87–118, https://doi.org/10.1016/j.tecto.2004.07.030.

Li, H., Wu, Q.H., Evans, N.J., Zhou, Z.K., Kong, H., Xi, X.S., and Lin, Z.W., 2018, Geochemistry and geochronology of the Banxi Sb deposit: Implications for fluid origin and the evolution of Sb mineralization in central-western Hunan, South China: Gondwana Research, v. 55, p. 112–134, https://doi.org/10.1016/j.gr.2017.11.010.

Li, H.T., Cao, D.Y., Wang, L.J., Guo, A.J., Li, Y.F., and Xu, H., 2013, Characteristics and evolution of coal-controlled structures on the east slope of the Xuefengshan domain in central Hunan Province [in Chinese with English abstract]: Geotectonica et Metallogenia, v. 37, p. 611–621.

Li, J.H., Zhang, Y.Q., Xian, X.B., Li, H.L., Dong, S.W., and Li, T.D., 2014, SHRIMP U-Pb dating of zircons from the Baimashan Longtan super-unit and Wawutang granites in Hunan Province and its geological implication: Journal of Jilin University: Earth Science Edition, v. 44, p. 158–175.

Li, S.S., 1996, Evolution of antimony mineralization by the mantle plume of deep fluid in Central Hunan: Hunan Geology, v. 15, p. 137–142 (in Chinese with English abstract).

Li, Z.M., 1993, Discussion on the ore genesis of the Xikuangshan Sb deposit [in Chinese]: Mineral Resource and Geology, v. 7, p. 88–93.

Li, Z.L., Hu, R.Z., Yang, J.S., Peng, J.T., Li, X.M., and Bi, X.W., 2007, He, Pb and S isotopic constraints on the relationship between the A-type Qitianling granite and the Furong tin deposit, Hunan Province, China: Lithos, v. 97, p. 161–173, https://doi.org/10.1016/j.lithos.2006.12.009.

Li, Z.X., and Li, X.H., 2007, Formation of the 1300-km-wide intracontinent orogen and post-orogenic magmatic province in Mesozoic South China: Geology, v. 35, p. 179–182, https://doi.org/10.1130/G23193A.1.

Lin, F.M., 2014, On the ore-forming fluid in the Xikuangshan antimony deposit, central Hunan [M.S. thesis]: Changsha, Center South University, p. 1–62 (in Chinese with English abstract).

Lin, Z.F., Zou, G.G., and Fu, B.Q., (1987) Geology of Sb deposits in central Hunan Province. Hunan Geology, v. supp.3, p. 1–33 (in Chinese with English abstract).

Lippolt, H.J., and Weigel, E., 1988, ^{4}He diffusion in ^{40}Ar-retentive minerals: Geochimica et Cosmochimica Acta, v. 52, no. 6, p. 1449–1458, https://doi.org/10.1016/0016-7037(88)90215-3.

Liu, G.M., and Jian, H.M., 1983, Geological characteristics of the Xikuangshan antimony ore field [in Chinese with English abstract]: Mineralium Deposita, v. 2, p. 43–49.

Liu, H.P., Zhang, Y.L., and Hu, W.Q., 1985, A study on the origin of the Xikuangshan antimony deposit [in Chinese with English abstract]: Hunan. Hunan Geology, v. 4, p. 28–39.

Liu, J.M., and Liu, J.J., 1997, Basin fluid genetic model of sediment-hosted micro-disseminated gold deposits in the gold-triangle area between Guizhou, Guangxi and Yunnan [in Chinese with English abstract]: Acta Mineralogica Sinica, v. 17, p. 448–456.

Liu, J.M., Ye, J., He, B.B., Zhang, R.B., and Li, Y.B., 2002, Sedex-type antimony deposits in giant antimony metallogenic belt, South China [in Chinese]: Mineralium Deposita, v. 21, p. 169–172.

Liu, J.M., Ye, J., Xu, J.H., and Shen, K., 2003, C-O and Sr-Nd isotopic geochemistry of carbonate minerals from gold deposits in East Shandong, China [in Chinese with English abstract]: Yanshi Xuebao, v. 19, p. 775–784.

Liu, J.Q., Xie, Y., Zhao, Z., Lin, J.S., Feng, W.M., and Huang, X.P., 2013, The geochronologic characteristics of Baimashan granite in western Hunan province and its geotectonic significance (in Chinese with English abstract): Earth Science Frontiers, v. 20, p. 25–35.

Liu, S.B., Wang, L.K., and Zhang, S., 1996, Review and discussion on C-O isotope tracing in hydrothermal (Au) ore deposits (in Chinese): Geology-Geochemistry, v. 4, p. 21–24.

Liu, W.J., 1992, Genesis of some antimony deposits in Southern China (in Chinese with English abstract): Journal of Chengdu College of Geology, v. 19, p. 10–19.

Lu, W.C., Cui, B.Q., Yang, S.Q., and Zhang, P., 1994, Strontium isotopic stratigraphic curve of the Devonian marine carbonates from Ganxi profile (in Chinese with English abstract): Acta Sedimentary Sinica, v. 12, p. 12–19.

Lu, X.W., Ma, D.S., Xie, Q.L., and Wang, W.Y., 2001, Trace element geochemical characteristics of Neoproterozoic–Paleozoic strata in western and central Hunan (in Chinese with English abstract): Geology-Geochemistry, v. 29, p. 24–30.

Lu, Y.L., Peng, J.T., Yang, J.H., Hu, A.X., Li, Y.K., Tan, H.Y., and Xiao, Q.Y., 2017, Petrogenesis of the Ziyunshan pluton in central Hunan, South China: Constraints from zircon U-Pb dating, element geochemistry and Hf-O isotopes (in Chinese with English abstract): Yanshi Xuebao, v. 33, p. 1705–1728.

Lupton, J.E., Baker, E.T., and Massoth, G.J., 1989, Variable ^{3}He/heat ratios in submarine hydrothermal systems: evidence from two plumes over the Juan de Fuca ridge: Nature, v. 337, p. 161–164, https://doi.org/10.1038/337161a0.

Lupton, J.E., Baker, E.T., Massoth, G.J., Thomson, R.E., Burd, B.J., Butterfield, D.A., Embley, R.W., and Cannon, G.A., 1995, Variations in water-column ^{3}He/heat ratios associated with the 1993 CoAxial event, Juan de Fuca Ridge: Geophysical Research Letters, v. 22, p. 155–158, https://doi.org/10.1029/94GL02797.

Ma, D.S., 1999, Regional pattern of element composition and fluid character in medium-low temperature metallogenic province of South China [in Chinese with English abstract]: Mineralium Deposita, v. 18, p. 347–358.

Ma, D.S., Pan, J.Y., Xie, Q.L., and He, J., 2002, Ore source of Sb (Au) deposits in Center Hunan: I. Evidences of trace elements and experimental geochemistry (in Chinese with English abstract): Mineralium Deposita, v. 3, p. 366–376.

Ma, D.S., Pan, J.Y., and Xie, Q.L., 2003, Ore sources of Sb (Au) deposits in Center Hunan: II. Evidence of isotopic geochemistry (in Chinese with English abstract): Mineralium Deposita, v. 21, p. 78–87.

Mao, J.W., Li, H.Y., Xu, J., and Luo, F.T., 1997, Geology and genesis of the Wangu Gold Deposit in Hunan Province, China: Beijing, Atomic Energy Publishing House, p.1–6 (in Chinese).

Mao, J.W., Cheng, Y.B., Chen, M.H., and Pirajno, F., 2013, Major types and time-space distribution of Mesozoic ore deposits in South China and their geodynamic settings: Mineralium Deposita, v. 48, p. 267–294, https://doi.org/10.1007/s00126-012-0446-z.

McDougall, I., and Harrison, T.M., 1988, Geochronology and thermochronology by the ^{40}Ar-^{39}Ar method: Oxford University Press, p. 1–212.

Niu, H.C., and Ma, D.S., 1991, Experimental geochemistry of gold, antimony and tungsten during water-rock interactions under low-temperature, open system (in Chinese with English abstract): Chinese Science Bulletin, v. 36, p. 1879–1881.

Ohmoto, H., 1986, Stable isotopes of ore deposits: Reviews in Mineralogy, v. 16, p. 491–560.

O'Neil, J.R., Clayton, R.N., and Mayeda, T.K., 1969, Oxygen isotope fractionation in divalent metal carbonates: The Journal of Chemical Physics, v. 51, p. 5547–5558, https://doi.org/10.1063/1.1671982.

Peng, J.T., and Hu, R.Z., 2001, Carbon and oxygen isotope systematics in the Xikuangshan giant antimony deposit, Central Hunan (in Chinese with English abstract): Dizhi Lunping, v. 47, p. 34–41.

Peng, J.T., Hu, R.Z., Deng, H.L., and Su, W.C., 2001, Strontium isotope geochemistry of the Xikuangshan antimony deposit, Central Hunan (in Chinese with English abstract): Geochimica, v. 30, p. 248–256.

Peng, J.T., Hu, R.Z., Zou, L.Q., and Liu, J.X., 2002, Isotopic tracing of ore-forming materials for Xikuangshan antimony deposit, center Hunan [in Chinese with English abstract]: Acta Mineralogica Sinica, v. 2, p. 155–159.

Peng, J.T., Hu, R.Z., and Burnard, P.G., 2003a, Samarium-Neodymium isotope systematics of hydrothermal calcites from the Xikuangshan antimony deposit (Hunan, China): The potential of calcite as a geochronometer: Chemical Geology, v. 200, p. 129–136, https://doi.org/10.1016/S0009-2541(03)00187-6.

Peng, J.T., Hu, R.Z., and Jiang, G.H., 2003b, Sm-Nd isotope systematics of fluorites from the Qinglong antimony deposit, Guizhou Province: Constraints on the mineralization timing and metal provenance (in Chinese with English abstract): Yanshi Xuebao, v. 19, p. 785–791.

Peng, J.T., Hu, R.Z., Qi, L., and Zhao, J.H., 2004, The REE distribution pattern of hydrothermal calcites from the Xikuangshan deposit and its constraint factors (in Chinese with English abstract): Dizhi Lunping, v. 50, p. 25–32.

Peng, J.T., Zhang, D.L., Hu, R.Z., Wu, M.J., and Lin, Y.X., 2008, Sm-Nd and Sr Isotope Geochemistry of Hydrothermal Scheelite from the Zhazixi W-Sb Deposit,Western Hunan (in Chinese with English abstract): Acta Geologica Sinica, v. 82, p. 1514–1521.

Peng, J.T., Zhang, D.L., Hu, R.Z., Wu, M.J., Liu, X.M., Qi, L., and Yu, Y.G., 2010, Inhomogeneous distribution of rare earth elements (REEs) in scheelite from the Zhazixi W-Sb deposit, western Hunan and its geological implications (in Chinese with English abstract): Dizhi Lunping, v. 56, p. 810–819.

Piepgras, D.J., and Wasserburg, G.J., 1985, Strontium and neodymium isotopes in hot springs on the East Pacific Rise and Guayamas Basin: Earth and Planetary Science Letters, v. 72, p. 341–356, https://doi.org/10.1016/0012-821X(85)90057-3.

Qiu, L., Yan, D.P., Tang, S.L., Wang, Q., Yang, W.X., Tang, X.L., and Wang, J.B., 2016, Mesozoic geology of southwestern China: Indosinian foreland overthrusting and subsequent deformation: Journal of Asian Earth Sciences, v. 122, p. 91–105, https://doi.org/10.1016/j.jseaes.2016.03.006.

Raczek, I., Jochum, K.P., and Hofmann, A.W., 2003, Neodymium and strontium isotope data for USGS reference materials BCR-1, BCR-2, BHVO-1, BHVO-2, AGV-1, AGV-2, GSP-1, GSP-2 and eight MPI-DING reference glasses: Geostandards Newsletter, v. 27, p. 173–179, https://doi.org/10.1111/j.1751-908X.2003.tb00644.x.

Rao, J.R., Luo, J.L., and Yi, Z.J., 1999, The mantle-crustal tectonic metallogenic model and ore-prospecting prognosis in the Xikuangshan antimony deposit (in Chinese with English abstract): Journal of Geophysical and Geochemical Exploration, v. 23, p. 241–249.

Sánchez, V., Cardellach, E., Corbella, M., Vindel, E., Martín-Crespo, T., and Boyce, A.J., 2010, Variability in fluid sources in the fluorite deposits from Asturias (N Spain): Further evidences from REE, radiogenic (Sr, Sm, Nd) and stable(S, C, O) isotope data: Ore Geology Reviews, v. 37, p. 87–100, https://doi.org/10.1016/j.oregeorev.2009.12.001.

Satish-Kumar, M., Hermann, J., Miyamoto, T., and Osanai, Y., 2010, Fingerprinting a multistage metamorphic fluid-rock history: Evidence from grain scale Sr, O and C isotopic and trace element variations in high-grade marbles from East Antarctica: Lithos, v. 114, p. 217–228, https://doi.org/10.1016/j.lithos.2009.08.010.

Savard, M.M., and Kontak, D.J., 1998, δ^{13}C-δ^{18}O-^{87}Sr/^{86}Sr covariations in ore-stage calcites at and around the Gays River Zn-Pb deposit (Nova Scotia, Canada)—Evidence for fluid mixing: Economic Geology and the Bulletin of the Society of Economic Geologists, v. 93, p. 818–833, https://doi.org/10.2113/gsecongeo.93.6.818.

Shi, M.K., Fu, B.Q., Jin, X.X., and Zhou, X.C., 1993, Antimony metallogeny in the central part of Hunan Province. Changsha: Hunan Publishing House of Science and Technology, p. 53–65 (in Chinese with English abstract).

Shu, L.S., 2006, Predevonian tectonic evolution of South China: From Cathaysian Block to Caledonian period folded orogenic belt (in Chinese with English abstract): Gaoxiao Dizhi Xuebao, v. 12, p. 418–431.

Shu, L.S., Zhou, X.M., Deng, P., Wang, B., Jiang, S.Y., Yu, J.H., and Zhao, X.X., 2009, Mesozoic tectonic evolution of the southeast China Block: New insights from basin analysis: Journal of Asian Earth Sciences, v. 34, p. 376–391, https://doi.org/10.1016/j.jseaes.2008.06.004.

Simmons, S.F., Sawkins, F.J., and Schlutter, D.J., 1987, Mantle-derived helium in two Peruvian hydrothermal ore deposits: Nature, v. 329, p. 429–432, https://doi.org/10.1038/329429a0.

Stuart, F.M., Turner, G., Duckworth, R.C., and Fallick, A.E., 1994, Helium isotopes as tracers of trapped hydrothermal fluids in ocean-floor sulfides: Geology, v. 22, p. 823–826, https://doi.org/10.1130/0091-7613(1994)022<0823:HIATOT>2.3.CO;2.

Stuart, F.M., Burnard, P.G., Taylor, R.P., and Turner, G., 1995, Resolving mantle and crustal contributions to ancient hydrothermal fluids: He-Ar isotopes in fluid inclusions from DaeHwa W-Mo mineralisation, South Korea: Geochimica et Cosmochimica Acta, v. 59, p. 4663–4673, https://doi.org/10.1016/0016-7037(95)00300-2.

Su, W.C., Hu, R.Z., Xia, B., Xia, Y., and Liu, Y.P., 2009, Calcite Sm-Nd isochron age of the Shuiyindong Carlin-type gold deposit, Guizhou, China: Chemical Geology, v. 258, p. 269–274, https://doi.org/10.1016/j.chemgeo.2008.10.030.

Tao, Y., Gao, Z.M., Jin, J.F., and Zeng, L.J., 2002, Ore-forming conditions of Xikuangshan-type antimony deposits in central Hunan (in Chinese with English abstract): Earth Science, v. 2, p. 184–195.

Tegengren, F.R., 1921, The His-K'uang-Shan antimony mining fields, Hsin-Hua district, Hunan district: Hunan Geology Survey Bulletin, v. 1, p. 1–26.

Thirlwall, M.F., 1991, Long-term reproducibility of multicollector Sr and Nd isotope ratio analysis: Chemical Geology, v. 94, p. 85–104, https://doi.org/10.1016/S0009-2541(10)80021-X.

Torgersen, T., Kennedy, B.M., and Hiyagon, H., 1989, Argon accumulation and the crustal degassing flux of ^{40}Ar in the Great Artesian Basin, Australia: Earth and Planetary Science Letters, v. 92, p. 43–56, https://doi.org/10.1016/0012-821X(89)90019-8.

Tu, G.C., 1984, Geochemistry of strata-bound deposits in China (Vol. 1). Beijing, Science Press, p. 129–188 (in Chinese with English abstract).

Turner, G., and Stuart, F.M., 1992, Helium/heat ratios and deposition temperatures of sulphides from the ocean floor: Nature, v. 357, p. 581–583, https://doi.org/10.1038/357581a0.

Turner, G., Burnard, P.G., Ford, J.L., Gilmour, J.D., Lyon, I.C., and Stuart, F.M., 1993, Tracing fluid sources and interaction: Philosophical Transactions of the Royal Society of London, v. 344, p. 127–140.

Veizer, J., 1989, Strontium isotopes in seawater through time: Annual Review of Earth and Planetary Sciences, v. 17, p. 141–167, https://doi.org/10.1146/annurev.ea.17.050189.001041.

Voicu, G., Bardoux, M., Stevenson, R., and Je'brak, M., 2000, Nd and Sr isotope study of hydrothermal scheelite and host rocks at Omai, Guiana Shield: Implications for ore fluid source and flow path during the formation of orogenic gold deposits: Mineralium Deposita, v. 35, p. 302–314, https://doi.org/10.1007/s001260050243.

Walters, W.J., Claypool, G.E., and Choquette, P.W., 1972, Reaction rate and δ^{18}O variation for the carbonate-phosphoric acid preparation method: Geochimica et Cosmochimica Acta, v. 89, p. 515–527.

Wang, H.C., Hsu, Y.T., and Liu, K.C., 1938, Record of antimony deposits. Hunan Geology Survey Memorial (Spec. A), v. 12, p. 1–182 (in Chinese).

Wang, K.X., Chen, P.R., Chen, W.F., Ling, H.F., Zhao, K.D., and Yu, Z.Q., 2012, Magma mingling and chemical diffusion in the Taojiang granitoids in the Hunan Province, China: Evidences from petrography, geochronology and geochemistry: Mineralogy and Petrology, v. 106, p. 243–264, https://doi.org/10.1007/s00710-012-0239-1.

Wang, Y.J., Fan, W.M., Sun, M., Liang, X., and Zhang, Y., 2007, Geochronological, geochemical and geothermal constraints on petrogenesis of the Indosinian peraluminous granites in the South China Block: A case study in the Hunan Province: Lithos, v. 96, p. 475–502, https://doi.org/10.1016/j.lithos.2006.11.010.

Wang, Y.J., Fan, W.M., Zhang, G.W., and Zhang, Y.H., 2013, Phanerozoic tectonics of the South China Block: Key observations and controversies: Gondwana Research, v. 23, p. 1273–1305, https://doi.org/10.1016/j.gr.2012.02.019.

Wei, W.F., Hu, R.Z., Bi, X.W., Jiang, G.H., Yan, B., Yin, R.S., and Yang, J.H., 2019, Mantle-derived and crustal He and Ar in the ore-forming fluids of the Xihuashan

granite-associated tungsten ore deposit, South China: Ore Geology Reviews, v. 105, p. 605–615, https://doi.org/10.1016/j.oregeorev.2019.01.014.

Wen, G.Z., Wu, Q., Liu, H.Y., Xie, G.Z., and Lei, X.L., 1993, Preliminary study on ore controlling regularities and metallogenic mechanism of the Xikuangshan superlarge antimony deposit (in Chinese with English abstract): Geology and Prospecting, v. 29, p. 20–27.

Wu, L.S., and Hu, X.W., 2000, Xikuangshan mica-plagioclase lamprophyre and its granite inclusions, Hunan Province (in Chinese with English abstract): Geology Geochemistry, v. 28, p. 51–55.

Wu, L.Y., Hu, R.Z., Peng, J.T., Bi, X.W., Jiang, G.H., Chen, H.W., Wang, Q.Y., and Liu, Y.Y., 2011, He and Ar isotopic compositions and genetic implications for the giant Shizhuyuan W-Sn-Bi-Mo deposit, Hunan Province, South China: International Geology Review, v. 53, p. 677–690, https://doi.org/10.1080/00206814.2010.510022.

Wu, L.Y., Hu, R.Z., Li, X.F., Sturt, F.M., Jiang, G.H., Qi, Y.Q., and Zhu, J.J., 2018, Mantle volatiles and heat contributions in high sulfidation epithermal deposit from the Zijinshan Cu-Au-Mo-Ag orefield, Fujian Province, China: Evidence from He and Ar isotopes: Chemical Geology, v. 480, p. 58–65, https://doi.org/10.1016/j.chemgeo.2017.08.005.

Wulff, K., Dziggel, A., Kolb, J., Vennemann, T., Böttcher, M.E., and Meyer, F.M., 2010, Origin of ore fluids of the sediment-hosted Navachab gold mine, Namibia: Constraints from Stable (O, H, C, S) isotopes: Economic Geology and the Bulletin of the Society of Economic Geologists, v. 105, p. 285–302, https://doi.org/10.2113/gsecongeo.105.2.285.

Xiao, Q.M., and Li, D.K., 1984, Study on the ore genesis of antimony deposits in Hunan Province (in Chinese with English abstract): Mineralium Deposita, v. 3, p. 13–25.

Xiao, X.G., 2014, Geochronology, ore geochemistry and genesis of the Banpo antimony deposit, Guizhou Province, China. PhD thesis, Kunming University of Science and Technology, Kunming, p. 1–138 (in Chinese with English abstract).

Xie, G.Q., Mao, J.W., Li, W., Fu, B., and Zhang, Z.Y., 2019, Granite-related Yangjiashan tungsten deposit, southern China: Mineralium Deposita, v. 54, p. 67–80, https://doi.org/10.1007/s00126-018-0805-5.

Xie, Q.L., 1996, Geochemistry of fluid geological process of mesothermal and epithermal hydrothermal deposits in Central and Western Hunan. Nanjing [unpublished Ph.D. dissertation]: Nanjing University, p. 50–60 (in Chinese with English abstract).

Yang, D.S., Shimizu, M., Shimazaki, H., Li, X.H., and Xie, Q.L., 2006, Sulfur isotope geochemistry of the supergiant Xikuangshan Sb deposit, central Hunan, China: Constraints on sources of ore constituents: Resource Geology, v. 56, p. 385–396, https://doi.org/10.1111/j.1751-3928.2006.tb00291.x.

Yang, R.Y., Ma, D.S., and Pan, J.Y., 2003, Geothermal field of ore-forming fluids of antimony deposits in Xikuangshan (in Chinese with English abstract): Geochimica, v. 23, p. 509–519.

Yang, Z.Z., Xie, Q.L., and Ma, D.S., 1998, The genesis and ore-forming fluid of the super-large antimony deposit of Xikuangshan, China (in Chinese with English abstract): Journal of Geology and Exploration, v. 13, p. 49–60.

Zeng, G.P., Gong, Y.J., Hu, X.L., and Xiong, S.F., 2017a, Geology, fluid inclusions, and geochemistry of the Zhazixi Sb-W deposit, Hunan, South China: Ore Geology Reviews, v. 91, p. 1025–1039, https://doi.org/10.1016/j.oregeorev.2017.08.001.

Zeng, G.P., Gong, Y.J., Wang, Z.F., Hu, X.L., and Xiong, S.F., 2017b, Structures of the Zhazixi Sb–W deposit, South China: Implications for ore genesis and mineral exploration: Journal of Geochemical Exploration, v. 182, p. 10–21, https://doi.org/10.1016/j.gexplo.2017.07.010.

Zhai, D.G., Mathur, R., Liu, S.A., Liu, J.J., Godfrey, L., Wang, K.X., Xu, J.W., and Vervoort, J., 2021, Antimony isotope fractionation in hydrothermal systems: Geochimica et Cosmochimica Acta, v. 306, p. 84–97, https://doi.org/10.1016/j.gca.2021.05.031.

Zhang, L.G., 1989, Diagenetic and Metallogenic Theory and Metallogenic Regularity: Beijing, Beijing Industry University Publish House, p. 121–123 [in Chinese with English abstract].

Zhang, L.G., Yao, J.Y., and Gu, X.P., 1998, Time and spatial distribution regularities and deposit types of antimony in China (in Chinese with English abstract): Mineral Resource and Geology, v. 12, p. 306–311.

Zhang, Z.Y., Xie, G.Q., Li, H.C., and Li, W., 2018, Preliminary study on muscovite 40Ar-39Ar geochronology and its significance of the Longshan Sb-Au deposit in Hunan Province (in Chinese with English abstract): Yanshi Xuebao, v. 34, p. 2535–2547.

Zhang, Z.Y., Xie, G.Q., Mao, J.W., Liu, W.G., Olin, P., and Li, W., 2019, Sm-Nd Dating and In-Situ LA-ICP-MS Trace Element Analyses of Scheelite from the Longshan Sb-Au Deposit, Xiangzhong Metallogenic Province, South China: Minerals (Basel), v. 9, p. 1–20, https://doi.org/10.3390/min9020087.

Zhao, J.H., Zhou, M.F., Yan, D.P., Zheng, J.P., and Li, J.W., 2011, Reappraisal of the ages of Neoproterozoic strata in South China: No connection with the Grenvillian orogeny: Geology, v. 39, p. 299–302, https://doi.org/10.1130/G31701.1.

Zhou, M.F., Yan, D.P., Kennedy, A.K., Li, Y.Q., and Ding, J., 2002, SHRIMP U-Pb zircon geochronological and geochemical evidence for Neoproterozoic arc-magmatism along the western margin of the Yangtze Block, South China: Earth and Planetary Science Letters, v. 196, p. 52–67, https://doi.org/10.1016/S0012-821X(01)00595-7.

Zhu, B.Q., 1997, Theory and application of isotope systematics in geological sciences: Beijing, Science Publishing House, p. 175–193 (in Chinese).

Zhu, Y.N., and Peng, J.T., 2015, Infrared microthermometric and noble gas isotope study of fluid inclusions in ore minerals at the Woxi orogenic Au-Sb-W deposit, western Hunan, South China: Ore Geology Reviews, v. 65, p. 55–69, https://doi.org/10.1016/j.oregeorev.2014.08.014.

Zhu, Z.Q., 2004, Research on the finite element numerical simulation of the geodynamic evolution features and characteristics of metallogenic in Hunan region since Mesozoic [Ph.D. thesis], Center South University, Changsha, p. 1–195 (in Chinese with English abstract).

Zou, T.X., 1988, Geochemica characteristics and ore-forming mechanism of the antimony ore field of Xikuangshan, Hunan (in Chinese with English abstract): Journal of Guilin College of Geology, v. 8, p. 187–195.

Science Editor: Wenjiao Xiao
Associate Editor: Shan Li

Manuscript Received 14 December 2021
Revised Manuscript Received 10 February 2022
Manuscript Accepted 11 April 2022

Printed in the USA